

Hyperfine structure of the hydroxyl free radical (OH) in electric and magnetic fields

Kenji Maeda¹, Michael L Wall², and Lincoln D Carr¹

¹Department of Physics, Colorado School of Mines, Golden, Colorado 80401, USA

²JILA, NIST and Department of Physics, University of Colorado, Boulder, CO 80309, USA

E-mail: kenji.bosefermi@gmail.com

Abstract. We investigate single-particle energy spectra of the hydroxyl free radical (OH) in the lowest electronic and rovibrational level under combined static electric and magnetic fields, as an example of heteronuclear polar diatomic molecules. In addition to the fine-structure interactions, the hyperfine interactions and centrifugal distortion effects are taken into account to yield the zero-field spectrum of the lowest $^2\Pi_{3/2}$ manifold to an accuracy of less than 2 kHz. We also examine level crossings and repulsions in the hyperfine structure induced by applied electric and magnetic fields. Compared to previous work, we found more than 10 percent reduction of the magnetic fields at level repulsions in the Zeeman spectrum subjected to a perpendicular electric field. It is important to take into account hyperfine structure when we investigate physics of OH molecules at micro-Kelvin temperatures and below.

1. Introduction

The hydroxyl free radical (OH molecule) is a simple but fascinating molecule in various fields of science; chemistry, astronomy, and physics. In chemistry, the OH molecule was the first short-lived molecule to be investigated by microwave spectroscopy and by gas-phase electron paramagnetic resonance (EPR) [1, 2], and was also the first free radical to be detected in a molecular beam [3]. In astronomy, it was found that the OH molecule was the first interstellar molecule detected at radio frequencies [4, 5]. The OH/IR stars, which exhibit OH line emission bright at near infrared wavelength, yielded so much intensity as OH sources that they led to an interpretation based on maser amplification, inspiring the concept of astrophysical masers [6]. In the field of cold and ultracold physics, the hydroxyl free radical has received a renewed attention as a constituent of quantum dipolar systems. A gas of OH molecules has been recently trapped and evaporatively cooled to milli-Kelvin temperatures at JILA [7].

Although there are many studies of the single-particle spectrum of the OH molecule in the context of chemistry and radio-astronomy as mentioned above, in the presence of electric and magnetic fields the energy spectra of OH have been calculated previously only to energy scales of milliKelvin temperatures (or frequencies of megaHertz) [7, 8, 9, 10, 11, 12, 13, 14, 15, 16], far from the sub-microKelvin temperatures at which OH molecules will become quantum degenerate. Therefore, as a necessary step towards a correct description of a quantum degenerate molecular dipolar gas of OH molecules at sub-microKelvin temperatures, we investigate its hyperfine structure in the lowest electronic and rovibrational states under combined electric and magnetic fields. In addition to the fine-structure interactions, we fully consider the hyperfine interactions and centrifugal distortion effects to obtain the zero-field spectrum of the lowest ${}^2\Pi_{3/2}$ manifold to an accuracy of less than 2 kHz \sim 100 nK. We also examine level crossings and repulsions in hyperfine structure in the presence of applied electric and magnetic fields to explore how these level crossings and repulsions change when we change the relative angle between the electric and magnetic fields.

Ahead of ultracold molecules, ultracold gases of atoms with magnetic dipole moments, or atomic dipolar gases, have been intensely investigated. Gases of Chromium [17], Dysprosium [18], and Erbium [19] have been trapped and cooled down to quantum degeneracy in experiments. Due to their anisotropic long-range dipole-dipole interactions, atomic dipolar gases are expected to exhibit novel quantum phenomena: spin textures [20, 21, 22], dipolar relaxation [23], Einstein-de Haas effects [24, 25] in their bosonic species, and ferronematic [26, 27] and antiferrosmectic-C phases [28] in their fermionic species. However, dipole-dipole interactions between atoms are fixed in strength by their permanent magnetic dipole moments. In contrast, polar molecules offer an electric dipole moment that is directly tunable via an applied electric field and can be made orders of magnitude larger than dipole moments in atoms. Cold and ultracold gases of molecules with electric dipole moments – molecular dipolar gases – are at or rapidly approaching quantum degeneracy in experiments, e.g., KRb [29], RbSr [30], OH [7], and SrF [31]. Recently, it has been shown that the single-particle spectrum and the dipole-dipole interactions of magnetic dipoles in a magnetic field can be simulated by symmetric top molecules subject to an electric field [32], and we stress that the hydroxyl radical (OH molecule), the subject of this article, also has the symmetric top structure in its electric dipole moment.

This paper is organized as follows. Section 2 is a preliminary section, overviewing a theoretical background of the OH free radical. In section 3, the hyperfine structure of OH is explored in the absence of external fields. We first introduce the effective Hamiltonian for the OH molecule and numerically diagonalize it to obtain the energy spectrum of OH in the lowest energy manifold. Section 4 deals

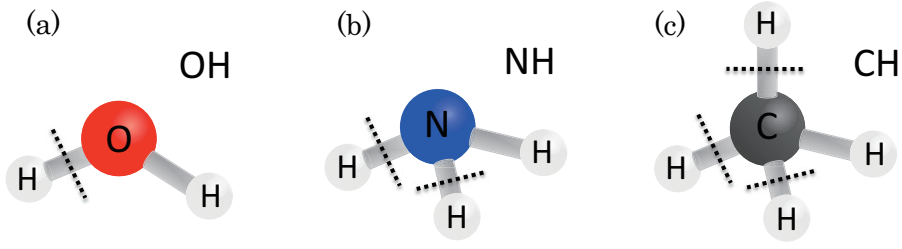


Figure 1. Free radicals: (a) OH, (b) NH, and (c) CH. The dotted lines represent dissociation of one or more hydrogen atoms to make free radicals from chemically stable, non-reactive, molecules.

with the effects of applied electric and magnetic fields, that is, the Stark and Zeeman effects in OH. We calculate the Stark and Zeeman spectra independently, and then examine the energy spectra in the presence of both electric and magnetic fields at relative angles of 0° , 45° , and 90° . We compare our results to previous work and show that the coupling with the excited states gives non-negligible contributions to the values of magnetic fields where level repulsions occur. Section 5 is devoted to the summary and concluding remarks. Appendix A summarizes definitions and formulae for the spherical tensor operators. Appendix B gives matrix elements of the effective Hamiltonian for OH in the Hund's case (a) basis.

2. Overview of the hydroxyl radical

We begin by introducing the hydroxyl (OH) free radical, for those readers who may be unfamiliar with it or find useful a reminder of its theoretical framework at higher temperatures ($\gtrsim 10^3$ K). The OH molecule can be obtained by dissociation of a hydrogen atom from a water molecule H_2O , as shown in Figure 1(a). Thus, the OH molecule has a chemically reactive, or radical, electron in its open shell. Other free radicals, like the NH and CH radicals shown in Figures 1(b) and (c), are also easily obtained from stable molecules, NH_3 (ammonia) and CH_4 (methane), respectively. Our model of the OH molecule is composed of an oxygen nucleus, a hydrogen nucleus, and nine electrons. The total kinetic energy operator is given by

$$\hat{T} = -\frac{\nabla_{\text{O}}^2}{2M_{\text{O}}} - \frac{\nabla_{\text{H}}^2}{2M_{\text{H}}} - \sum_{i=1}^9 \frac{\nabla_i^2}{2m_e}. \quad (1)$$

Here M_{O} , M_{H} , and m_e are masses of the oxygen nucleus, hydrogen nucleus, and electron, respectively, and ∇_{O} , ∇_{H} , and ∇_i are gradient operators with respect to the coordinates of the oxygen nucleus \mathbf{r}_{O} , hydrogen nucleus \mathbf{r}_{H} , and electrons \mathbf{r}_i , respectively. Throughout this paper, we shall choose units such that $\hbar = 1$ unless quoting an energy in frequency units. Setting the center of mass of the oxygen nucleus and hydrogen nucleus as the origin of the coordinate system, we rewrite the kinetic energy operator as

$$\hat{T} = -\frac{\nabla_{\text{M}}^2}{2M} - \frac{\nabla_{\text{r}}^2}{2m} - \sum_{i=1}^9 \frac{\nabla_i'^2}{2m_e} - \frac{1}{2(M_{\text{O}} + M_{\text{H}})} \sum_{i,j=1}^9 \nabla_i' \cdot \nabla_j', \quad (2)$$

with the total mass of the molecule $M = M_{\text{O}} + M_{\text{H}} + 9m_e$ and the reduced mass of the two nuclei $m = M_{\text{O}}M_{\text{H}}/(M_{\text{O}} + M_{\text{H}})$. Note that ∇_{M} , ∇_{r} , and ∇_i' are gradient operators with respect to the center of mass coordinate of the molecule $\mathbf{r}_{\text{M}} = (M_{\text{O}}\mathbf{r}_{\text{O}} + M_{\text{H}}\mathbf{r}_{\text{H}} + \sum_{i=1}^9 m_e\mathbf{r}_i)/M$, the relative coordinate of two nuclei $\mathbf{r} = \mathbf{r}_{\text{H}} - \mathbf{r}_{\text{O}}$, and electron coordinates \mathbf{r}_i' measured from the center of mass of the two nuclei. For the relative motion of the oxygen nucleus and hydrogen nucleus \mathbf{r} , we use the polar coordinate

representation (r, θ, ϕ) , which gives

$$\hat{T} = -\frac{\nabla_{\mathbf{M}}^2}{2M} - \frac{1}{2mr^2} \frac{\partial}{\partial r} \left(r^2 \frac{\partial}{\partial r} \right) + \frac{1}{2mr^2} \hat{\mathbf{R}}^2 - \sum_{i=1}^9 \frac{\nabla_i'^2}{2m_e} - \frac{1}{2(M_{\text{O}} + M_{\text{H}})} \sum_{i,j=1}^9 \nabla_i' \cdot \nabla_j', \quad (3)$$

with the square of the rotational angular momentum operator of two nuclei given by

$$\hat{\mathbf{R}}^2 = -\frac{1}{\sin \theta} \frac{\partial}{\partial \theta} \left(\sin \theta \frac{\partial}{\partial \theta} \right) - \frac{1}{\sin^2 \theta} \frac{\partial^2}{\partial \phi^2}. \quad (4)$$

The first term in Eq. (3) represents the translational motion of the molecule, that will be neglected in our single molecule study, the second and third terms describe the radial and rotational motion of two nuclei related to vibration and rotation of the molecule, and the fourth and fifth terms are the kinetic energy operators of the electrons and the mass polarization term, respectively. Due to the large mass difference between electrons and nuclei, $m_e \ll M_{\text{O}}, M_{\text{H}}$, we will neglect the mass polarization term and define the electronic Hamiltonian of the OH molecule with the Coulombic potential as

$$\hat{H}_{\text{el}} = -\sum_{i=1}^9 \frac{\nabla_i'^2}{2m_e} + \frac{e^2}{4\pi\epsilon_0} \left\{ \sum_{i<j} \frac{1}{r_{ij}} - \sum_{i=1}^9 \left(\frac{Z_{\text{O}}}{r_{\text{O}i}} + \frac{Z_{\text{H}}}{r_{\text{H}i}} \right) + \frac{e^2 Z_{\text{O}} Z_{\text{H}}}{4\pi\epsilon_0 r} \right\}, \quad (5)$$

where r_{ij} is the distance between electrons i and j , and $r_{\text{O}i}$ ($r_{\text{H}i}$) is the distance between the electron i and the oxygen nucleus (hydrogen nucleus). The electric charges of electrons, the oxygen nucleus and hydrogen nucleus are e , $Z_{\text{O}}e$, and $Z_{\text{H}}e$, respectively, and ϵ_0 is the permittivity of vacuum. Since we included the Coulombic potential between the oxygen nucleus and hydrogen nucleus in the electronic Hamiltonian, the nuclear Hamiltonian of the OH molecule is just given by the kinetic energy operator of the relative motion of the nuclei

$$\hat{H}_{\text{nuc}} = -\frac{1}{2mr^2} \frac{\partial}{\partial r} \left(r^2 \frac{\partial}{\partial r} \right) + \frac{1}{2mr^2} \hat{\mathbf{R}}^2. \quad (6)$$

Using a singular perturbation method in terms of a mass-ratio parameter $(m_e/m)^{1/4}$, Born and Oppenheimer [33] showed that in a typical molecule $\Delta E_{\text{vib}}/\Delta E_{\text{el}} \approx \Delta E_{\text{rot}}/\Delta E_{\text{vib}} \approx (m_e/m)^{1/2}$, where ΔE_{el} , ΔE_{vib} , and ΔE_{rot} are the energetic separations between the ground state and the first excited state in electronic, vibrational, and rotational energy levels, respectively[‡]. This general result separates electronic and nuclear motions in a molecule and allows us to solve the Schrödinger equation for electrons in the presence of the electrostatic field produced by fixed nuclear charges,

$$\hat{H}_{\text{el}} \psi_{\text{el}}^{(n)} = E_{\text{el}}^{(n)} \psi_{\text{el}}^{(n)}. \quad (7)$$

Here we note that since the internuclear distance r is fixed in Eq. (7) the resultant eigenvalues $\{E_{\text{el}}^{(n)}(r)\}_n$ and eigenfunctions $\{\psi_{\text{el}}^{(n)}(\mathbf{r}'_1, \dots, \mathbf{r}'_9; r)\}_n$ depend on r parametrically. For the Schrödinger equation of the whole OH molecule,

$$(\hat{H}_{\text{el}} + \hat{H}_{\text{nuc}})\Psi = E\Psi, \quad (8)$$

we assume a partial separation of variables of the molecular wave function in the form of

$$\Psi(\mathbf{r}'_1, \dots, \mathbf{r}'_9, r, \theta, \phi) = \sum_n \psi_{\text{el}}^{(n)}(\mathbf{r}'_1, \dots, \mathbf{r}'_9; r) \chi^{(n)}(r, \theta, \phi). \quad (9)$$

[‡] A simple estimate is as follows [34]. From the uncertainty principle, in a molecule of size a electrons have momenta typically of \hbar/a , and we have $\Delta E_{\text{el}} \sim \hbar^2/(2m_e a^2)$. The vibrational motion of nuclei distorts the electron wave functions, and its approximate harmonic oscillator potential $m\omega^2 a^2/2$ should be on the order of the electronic excitation energy, which gives the typical frequency of the vibration $\omega \sim (m_e/m)^{1/2} \hbar/(m_e a^2)$. The nuclear vibration is thus spaced in energy by $\hbar\omega$, which gives the relation $\Delta E_{\text{vib}}/\Delta E_{\text{el}} \sim (m_e/m)^{1/2}$. Finally, the rotational energy of nuclei with angular momentum $\hbar N$ is estimated as $\hbar^2 N(N+1)/(2I)$ with the moment of inertia of nuclei $I \sim ma^2$, yielding $\Delta E_{\text{rot}}/\Delta E_{\text{vib}} \sim (m_e/m)^{1/2}$.

We defined the nuclear part of the molecular wave function by $\chi^{(n)}$. Then the molecular Schrödinger equation, Eq. (8), reduces to

$$\left(\frac{\hat{p}_r^2}{2m} + \frac{1}{2mr^2} \hat{\mathbf{R}}^2 + E_{\text{el}}^{(n)} - E \right) \chi^{(n)} = \sum_m \hat{K}_{mn} \chi^{(m)}, \quad (10)$$

with matrix elements \hat{K}_{mn} which couple different electronic states,

$$\hat{K}_{mn} = \int d\mathbf{r}_1 \cdots d\mathbf{r}_9 \psi_{\text{el}}^{(m)*} \left\{ \frac{1}{m} \left(\hat{p}_r \psi_{\text{el}}^{(n)} \right) \hat{p}_r + \frac{1}{2m} \left(\hat{p}_r^2 \psi_{\text{el}}^{(n)} \right) \right\}, \quad (11)$$

where \hat{p}_r is the momentum operator conjugate to r ,

$$\hat{p}_r = \frac{1}{ir} \frac{\partial}{\partial r}. \quad (12)$$

In the *Born-Oppenheimer approximation*, which corresponds to the lowest order approximation in $(m_e/m)^{1/2}$ [33, 34], all the matrix elements \hat{K}_{mn} are set to be zero, and $\chi^{(n)}$ becomes an eigenfunction of

$$\left(\frac{\hat{p}_r^2}{2m} + \frac{1}{2mr^2} \hat{\mathbf{R}}^2 + E_{\text{el}}^{(n)} \right) \chi^{(n)} = E \chi^{(n)}, \quad (13)$$

where $E_{\text{el}}^{(n)}$ can be considered as an *adiabatic potential* for the vibration of nuclei in a given electronic state.

Even if we fix the internuclear distance, the electronic Schrödinger equation (7) cannot be solved exactly. Therefore, we usually model the exact solutions of Eq. (7) using the electron wave functions in an isolated oxygen atom and those in an isolated hydrogen atom. This ansatz is called the *linear combination of atomic orbitals (LCAO) method* since the electron wave functions in the molecule are modeled by linear combinations of the electron wave functions in the parent atoms, called *atomic orbitals*. We shall start from a review on atomic orbitals for the sake of completeness. The wave functions of an electron in the hydrogen atom are given by $\psi_{n\ell m_\ell}^{\text{H}}(\mathbf{r}_1) = R_{n\ell}(r_1) Y_{\ell m_\ell}(\theta_1, \phi_1)$ with the associated Laguerre functions $R_{n\ell}$ and spherical harmonics $Y_{\ell m_\ell}$. The quantities n , ℓ , and m_ℓ are the principal, azimuthal, and magnetic quantum numbers, respectively, having the allowed values: $n \in \mathbb{N}$, $\ell = 0, 1, 2, \dots, n-1$, and $m_\ell = 0, \pm 1, \pm 2, \dots, \pm \ell$. The electron wave functions $\psi_{n\ell m_\ell}^{\text{H}}$ are known as atomic orbitals, and for $\ell = 0, 1, 2, 3, \dots$, they are referred as *s*, *p*, *d*, *f* orbitals, respectively. The values of the principal quantum numbers n are specified as prefixes, *1s*, *2s*, *2p*, *3s*, *3p*, *3d*, and so forth. As for the magnetic quantum numbers m_ℓ , we take real linear combinations of the complex wave functions $\psi_{n\ell m_\ell}^{\text{H}}$ with different values of m_ℓ . For example, we define $\psi_{2p_x}^{\text{H}} = (\psi_{2,1,1}^{\text{H}} + \psi_{2,1,-1}^{\text{H}})/\sqrt{2}$ and $\psi_{2p_y}^{\text{H}} = -i(\psi_{2,1,1}^{\text{H}} - \psi_{2,1,-1}^{\text{H}})/\sqrt{2}$, and call them *2p_x* and *2p_y* orbitals because they are real functions and have their maxima along *x*- and *y*-directions, respectively. The *2p_z* orbital is given by $\psi_{2p_z}^{\text{H}} = \psi_{2,1,0}^{\text{H}}$ since the wave function $\psi_{2,1,0}^{\text{H}}$ is a real function with its maximum along the *z*-axis. On the other hand, the electron wave functions, or atomic orbitals, of the oxygen atom cannot be given exactly since we cannot analytically solve the Schrödinger equation for eight electrons interacting with each other via the Coulombic potential. Then we usually consider the *Hartree-Fock variational state* $\psi_{\text{HF}}^{\text{O}}$ [35, 36, 37, 38] composed of a simple product of one-electron wave functions ϕ_i , also called *orbitals*, and fully antisymmetrized with respect to interchange of any two electrons,

$$\psi_{\text{HF}}^{\text{O}}(\mathbf{r}_1, s_1, \mathbf{r}_2, s_2, \dots, \mathbf{r}_8, s_8) = \frac{1}{\sqrt{8!}} \sum_{\sigma \in \mathfrak{S}_8} \text{sgn}(\sigma) \phi_{\sigma(1)}(\mathbf{r}_1, s_1) \phi_{\sigma(2)}(\mathbf{r}_2, s_2) \cdots \phi_{\sigma(8)}(\mathbf{r}_8, s_8), \quad (14)$$

where \mathfrak{S}_8 stands for the symmetric group of eight elements and $\text{sgn}(\sigma)$ is the sign of the permutation σ taking its value 1 and -1 for even and odd permutations, respectively. Note here that we specify

components of the spin-1/2 spinors of electrons by $s_i = \pm 1/2$, assuming that one-electron wave functions can be decomposed into $\phi_i(\mathbf{r}_i, s_i) = \varphi_i(\mathbf{r}_i)\chi_i(s_i)$ with spatial orbitals φ_i and spin orbitals χ_i . Minimizing the energy expectation in $\psi_{\text{HF}}^{\text{O}}$ subject to the condition that $\{\phi_i\}_{i=1}^8$ is an orthonormal set gives the coupled nonlinear equations for the oxygen atomic orbitals,

$$\begin{aligned}
 & \left(-\frac{\nabla_i^2}{2m_e} - \frac{Z_{\text{O}}e^2}{4\pi\epsilon_0} \frac{1}{|\mathbf{r}_i|} + \sum_{j \neq i} \sum_{s_j = \pm 1/2} \int d\mathbf{r}_j \frac{e^2}{4\pi\epsilon_0} \frac{|\phi_j(\mathbf{r}_j, s_j)|^2}{|\mathbf{r}_i - \mathbf{r}_j|} \right) \phi_i(\mathbf{r}_i, s_i) \\
 & - \sum_{j \neq i} \sum_{s_j = \pm 1/2} \int d\mathbf{r}_j \frac{e^2}{4\pi\epsilon_0} \frac{1}{|\mathbf{r}_i - \mathbf{r}_j|} \phi_j^*(\mathbf{r}_j, s_j) \phi_j(\mathbf{r}_i, s_i) \phi_i(\mathbf{r}_j, s_j) = \varepsilon_i \phi_i(\mathbf{r}_i, s_i), \quad (15)
 \end{aligned}$$

which are called the *Hartree-Fock equations*. The Hartree-Fock equations (15) consist of, in order, the kinetic energy of an electron, the Coulombic potential between the electrons and the oxygen nucleus, the averaged repulsions from the other electrons, the so-called *exchange potential* arising from the antisymmetrization in $\psi_{\text{HF}}^{\text{O}}$, or from the Pauli exclusion principle in electrons, and the energy of the orbital ϕ_i . Numerical solutions of the Hartree-Fock equations (15), usually obtained by iteration, supports the *shell model of atoms*. The shell model has the following major features: (i) the quantum numbers of atomic orbitals are given by n, ℓ, m_ℓ like in the hydrogen atom, and also by spin quantum number m_s , i.e., $\phi_i(\mathbf{r}_i, s_i) = \varphi_{n\ell m_\ell}(\mathbf{r}_i)\chi_{m_s}(s_i)$; and (ii) the energy of the orbital ε_i depends on n and ℓ due to the deviation from a pure $1/r$ -potential, but not on m_ℓ and m_s , thus we have $4\ell + 2$ degenerate orbitals for given values of n and ℓ . This set of $4\ell + 2$ orbitals is called a *shell*, and the distribution of electrons in these shells is called the *electron configuration*.

Next we discuss the qualitative nature of the electron wave functions of molecules, called *molecular orbitals*. According to the LCAO method, the OH molecule has the molecular orbitals and their energy levels for electrons, as shown in Figure 2(a). The $1s$ and $2s$ atomic orbitals of the oxygen atom are energetically far separated from the $1s$ atomic orbital of the hydrogen atom, and only the $2p$ atomic orbitals of the oxygen atom can couple with the $1s$ atomic orbital of the hydrogen atom. Among the $2p$ atomic orbitals of the oxygen atom, the $2p_z$ orbital has overlap with the $1s$ atomic orbital of the hydrogen atom, while the $2p_x$ and $2p_y$ orbitals do not have overlap in spatial average and they are renamed as $2p\pi$ molecular orbitals. Then, the $2p_z$ orbital of the oxygen atom and $1s$ orbital of the hydrogen atom interact in-phase to form a bonding molecular orbital $2p\sigma$, or out-of-phase to form an antibonding molecular orbital $2p\sigma^*$. Note that in the σ and π molecular orbitals, an electron has the projection of orbital angular momentum along the internuclear axis 0 and ± 1 , respectively. Thus, the lowest energy electron configuration of the OH molecule, called the $X^2\Pi$ state, is given by

$$X^2\Pi : (1s)^2(2s\sigma)^2(2p\sigma)^2(2p\pi)^3, \quad (16)$$

as shown in Figure 2(b), and the first excited electronic state, called the $A^2\Sigma$ state, becomes

$$A^2\Sigma : (1s)^2(2s\sigma)^2(2p\sigma)^1(2p\pi)^4, \quad (17)$$

as shown in Figure 2(c). Here the superscripts of the braces represent the numbers of electrons occupied taking into account electronic spin degrees of freedom. Defining Λ as the projection of electronic orbital angular momentum along the symmetry axis of the molecule, we have $\Lambda = \pm 1$ in the $X^2\Pi$ electronic state, while $\Lambda = 0$ in the $A^2\Sigma$ electronic state. The two-fold degeneracies in states with $|\Lambda| \neq 0$ are called *Λ -doubling*, which comes from the fact that the Hamiltonian of a diatomic molecule is invariant under a reflection with respect to a plane containing the symmetry axis of the molecule while Λ changes its sign under such reflection. The electronic ground $X^2\Pi$ state and the first excited $A^2\Sigma$ state are

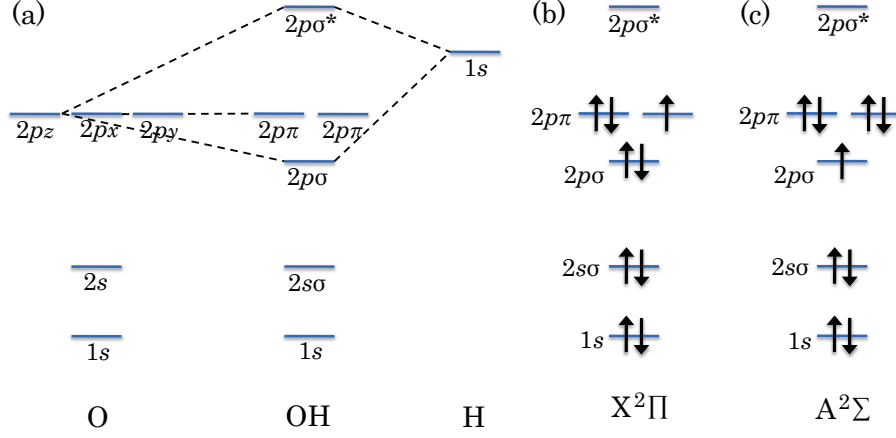


Figure 2. (a) Energy level diagram of electrons in OH molecule based on the LCAO method. (b) Electronic configuration in the $X^2\Pi$ ground state, and (c) in the first excited $A^2\Sigma$ state of OH molecule, where the up and down arrows occupying the molecular orbitals denote electrons with spin quantum numbers $1/2$ and $-1/2$, respectively.

far separated from each other by $4\text{ eV} \sim 10^3\text{ THz} \sim 5 \times 10^4\text{ K}$, which is the largest energy scale in the hierarchy of energy levels. Fuller details on electronic structures of molecules can be found in [39].

Now the electronic structures in the molecule become input parameters of the nuclear Schrödinger equation (13). Since in the Born-Oppenheimer approximation there is no mixing of different electronic states, we can write down the ground state of the OH molecule as $\Psi = \psi_{el}^{(X^2\Pi)} \chi^{(X^2\Pi)}$, and the nuclear wave function $\chi^{(X^2\Pi)}$ is determined by Eq. (13) with the $X^2\Pi$ adiabatic potential $E^{(X^2\Pi)}$. Noting that there is the hierarchy in energy, $\Delta E_{\text{rot}}/\Delta E_{\text{vib}} \approx (m_e/m)^{1/2}$, we can first investigate the vibrational motion assuming that the rotational motion of nuclei is frozen out. For a stable molecule the electron configuration of the ground state supports the chemical bond of the molecule, and therefore the adiabatic potential $E^{(X^2\Pi)}$ should have its minimum at the *equilibrium distance* r_0 of the nuclei. Employing the *harmonic approximation*, that is, replacing $E^{(X^2\Pi)}$ by the first two terms in a power series expansion about $r = r_0$, we extract the vibrational motion from Eq. (13),

$$-\frac{1}{2mr} \frac{d^2}{dr^2} \{r f_v(r)\} + \frac{1}{2} k(r - r_0)^2 f_v(r) = E_v f_v(r), \quad (18)$$

where k is a curvature given by the harmonic approximation $E^{(X^2\Pi)}(r) \simeq k(r - r_0)^2/2$. We can analytically solve Eq. (18) to obtain the eigenfunctions $f_v(r) = c_v r H_v(\tilde{r}) e^{-\tilde{r}^2/2}$ and eigenenergies $E_v = (v+1/2)\omega_{\text{vib}}$, where H_v is the Hermite polynomial with vibrational quantum number $v = 0, 1, 2, \dots$, and the harmonic vibrational frequency is given by $\omega_{\text{vib}} = \sqrt{k/m}$. We also defined a dimensionless variable $\tilde{r} = \sqrt{m\omega_{\text{vib}}}(r - r_0)$ and a normalization constant c_v .

For the rest of the motion in Eq. (13), the rotational motion of nuclei, we assume that the internuclear distance is fixed to the equilibrium or average value r_0 . Then, the rotational motion of nuclei reduces to motion of a *rigid rotor*

$$\frac{\hat{\mathbf{R}}^2}{2mr_0^2} Y_{R,M_R}(\theta, \phi) = E_{R,M_R} Y_{R,M_R}(\theta, \phi), \quad (19)$$

which immediately gives the spherical harmonics Y_{R,M_R} as eigenfunctions and their eigenenergies as $E_{R,M_R} = R(R+1)/(2mr_0^2)$ where $R = 0, 1, 2, \dots$ and $M_R = 0, \pm 1, \pm 2, \dots, \pm R$. Note that due to centrifugal forces of rotational motion the internuclear distance will increase from r_0 as the molecule rotates faster. This modifies the moment of inertia in Eq. (18) and gives corrections to the

rigid rotor energies, called *centrifugal distortion corrections*§. It is in part the centrifugal distortion corrections which are vital to include in order to reach 100 nK precision for the OH molecule. Treating nuclear motion under the harmonic oscillator and rigid rotor approximations, we can write down the nuclear wave functions in the electronic ground state as $\chi_{v,R,M_R}^{(X^2\Pi)}(r, \theta, \phi) = f_v(r)Y_{R,M_R}(\theta, \phi)$ with their eigenenergies $E_{v,R,M_R} = (v + 1/2)\omega_{\text{vib}} + R(R + 1)/(2mr_0^2)$.

In addition to the electrostatic Coulombic potentials, molecular Hamiltonians have a lot of microscopic terms which explain relativistic effects, fine and hyperfine structure, e.g., there are 27 terms derived for general diatomic molecules in [40] including electronic spin-spin, spin-orbit couplings and electronic spin-nuclear spin coupling. Such microscopic interactions give energy scales comparable to thermal energies in cold and ultracold temperatures (10 mK – 10 nK), while the above electronic and vibrational motions corresponds to much higher temperatures, 10^4 K and 10^3 K, respectively. Thus for the purpose of cold and ultracold physics, it is convenient to derive an *effective Hamiltonian* which operates only within nuclear rotational, electronic spin, and nuclear spin degrees of freedom in the vibrational and electronic (*vibronic*) ground state. Such an effective Hamiltonian is obtained by including the effects of off-diagonal matrix elements in the original Hamiltonian which couple the vibronic ground state to other excited states. Suppose that our full Hamiltonian can be divided into a dominant part \hat{H}_0 and perturbative part $\lambda\hat{H}_1$ with a perturbation parameter λ ,

$$\hat{H} = \hat{H}_0 + \lambda\hat{H}_1 . \quad (20)$$

In the molecule, \hat{H}_0 is composed of the non-relativistic kinetic energy operators of electrons, the vibrational terms of nuclei, and the electrostatic Coulombic potentials, while $\lambda\hat{H}_1$ is composed of all the remaining terms, nuclear rotation, electronic spin-spin, spin-orbit couplings and electronic spin-nuclear spin coupling, and so on. The eigenstates of \hat{H}_0 are purely vibronic eigenstates,

$$\hat{H}_0 |\eta; k\rangle_0 = E_\eta^0 |\eta; k\rangle_0 , \quad (21)$$

where η denotes the vibronic quantum numbers and k represents nuclear rotational, electronic spin, and nuclear spin quantum numbers. The perturbative term $\lambda\hat{H}_1$ mixes these quantum numbers and the eigenstates of \hat{H} are given by

$$\hat{H} |\bar{\eta}; \bar{k}\rangle = E_{\bar{\eta};\bar{k}} |\bar{\eta}; \bar{k}\rangle . \quad (22)$$

Here we used *adiabatic labels* $\bar{\eta}$ and \bar{k} assuming that the state $|\bar{\eta}; \bar{k}\rangle$ coincides with $|\eta; k\rangle_0$ when we adiabatically turn off the perturbative term. The effective Hamiltonian \hat{H}_{eff} of our interest should act only on a subspace \mathcal{H}_{eff} spanned by the vibronic ground states $\{|0; k\rangle_0\}_k$ of \hat{H}_0 , while reproducing the eigenenergies $\{E_{\bar{0};\bar{k}}\}_{\bar{k}}$ of the full Hamiltonian. Therefore, the effective Hamiltonian should satisfy an eigenvalue equation such that

$$\hat{H}_{\text{eff}} |0; \bar{k}\rangle_{\text{eff}} = E_{\bar{0};\bar{k}} |0; \bar{k}\rangle_{\text{eff}} , \quad (23)$$

with eigenstates $|0; \bar{k}\rangle_{\text{eff}}$ given by linear combinations of states only in \mathcal{H}_{eff} . This condition gives a perturbative expansion of \hat{H}_{eff} as

$$\hat{H}_{\text{eff}} = \hat{H}_0 + \lambda\hat{P}_0\hat{H}_1\hat{P}_0 + \lambda^2\hat{P}_0\hat{H}_1\frac{\hat{Q}_0}{E_0^0 - \hat{H}_0}\hat{H}_1\hat{P}_0 + \mathcal{O}(\lambda^3) , \quad (24)$$

§ We can get an insight into centrifugal distortion corrections based on classical mechanics [40]. Suppose that in the rotating molecule with its angular velocity ω , the internuclear distance increases to r_{CD} which is determined by the requirement that the centrifugal force $m\omega^2 r_{\text{CD}}$ is balanced by the restoring force $k(r_{\text{CD}} - r_0)$, that is, $r_{\text{CD}} = [1 + m\omega^2/(k - m\omega^2)]r_0$. The rotational energies are modified to $E = R_{\text{cl}}^2/(2mr_{\text{CD}}^2) + k(r_{\text{CD}} - r_0)^2/2$ where $R_{\text{cl}} = mr_{\text{CD}}^2 \omega$ is the classical angular momentum. Assuming the stiffness of the molecule ($k \gg m\omega^2$), we obtain $E \simeq R_{\text{cl}}^2/(2mr_0^2) - R_{\text{cl}}^4/(2mr_0^6 k)$ to the lowest order in $m\omega^2/k$, and the term proportional to R_{cl}^4 is a centrifugal distortion correction.

where \hat{P}_0 is a projection operator onto the subspace \mathcal{H}_{eff} and \hat{Q}_0 is a projection operator onto its orthogonal complement,

$$\hat{P}_0 = \sum_i |0; i\rangle_{00} \langle 0; i|, \quad (25)$$

$$\hat{Q}_0 = \mathbf{1} - \hat{P}_0 = \sum_{\eta \neq 0} \sum_i |\eta; i\rangle_{00} \langle \eta; i|. \quad (26)$$

A detailed derivation and fuller expression for Eq. (24) can be found in [40]. The first and second terms in Eq. (24) are just the direct projection of the full Hamiltonian onto the subspace of the vibronic ground states without perturbation. The third term in Eq. (24) gives the effects of coupling between the vibronic ground and excited states. It should be remarked that the Λ -doubling degeneracies are broken (*Λ -doubling splitting*) by the admixture of the rotational levels in the $X^2\Pi$ state with the corresponding levels of the $A^2\Sigma$ state via electronic spin-orbit interaction and the nuclear rotational-electronic orbit interaction [41]. This is because each rotational level of the $A^2\Sigma$ state has a definite parity with respect to spatial inversion, either positive or negative, and thus interacts with only one of the two parity states in the $X^2\Pi$ state. Also, the centrifugal distortion corrections are obtained by the admixture of the vibrational ground and excited states.

Throughout this paper, we will employ the effective Hamiltonian for the OH molecule acting on rotational, fine and hyperfine levels in its vibronic ground state and investigate its energy levels in the presence of electric and magnetic fields.

3. Hyperfine structure of OH molecule without external fields

In a study of molecular spectroscopy, especially at low temperatures where vibrational degrees of freedom for nuclei are frozen out, we often use a quantum rotor model, replacing a molecule by a quantum-mechanically rotating rigid body with several angular momenta [40, 42]. The quantum rotor model takes into account not only the rotation but also interactions between angular momenta, depending on the species of molecule. Since the OH molecule in its electronic ground state is a diatomic molecule with a nuclear spin of $I = 1/2$ and has an electron in the open $2p$ -shell, there are four main kinds of angular momenta: the rotational angular momentum of the nuclei $\hat{\mathbf{R}}$, the electronic orbital angular momentum $\hat{\mathbf{L}}$, the electronic spin angular momentum $\hat{\mathbf{S}}$, and the nuclear spin angular momentum $\hat{\mathbf{I}}$, see Figure 3. Furthermore, the total angular momentum without the nuclear spin is conventionally defined as $\hat{\mathbf{J}} = \hat{\mathbf{R}} + \hat{\mathbf{L}} + \hat{\mathbf{S}}$, and the geometric part of angular momenta as $\hat{\mathbf{N}} = \hat{\mathbf{R}} + \hat{\mathbf{L}}$. Here we remark that for the OH molecule in its $^2\Pi$ states the magnitudes of the angular momenta $\hat{\mathbf{L}}$, $\hat{\mathbf{S}}$, and $\hat{\mathbf{I}}$ are fixed to be $L = 1$, $S = 1/2$, and $I = 1/2$, respectively, while the rotational quantum number R takes non-negative integer values. In this section, we review the quantum rotor model of the OH molecule in the absence of external fields, and then numerically calculate its energy spectrum including hyperfine structure, leading to the lowest 16 states and therefore reproducing experimental data to an accuracy of 2 kHz. Appendix A summarizes definitions of spherical tensor operators and their formulae, which we utilize in calculations of matrix elements throughout this paper.

3.1. The zero-field effective Hamiltonian for OH

We first summarize the zero-field effective Hamiltonian for the OH molecule in the $v = 0$ level of the $X^2\Pi$ state. Throughout this paper, we use notations in molecular spectroscopy to represent the

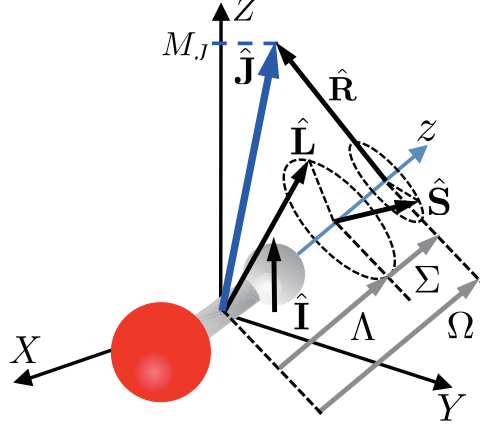


Figure 3. Vector coupling diagram for OH molecule in Hund's case (a) basis (red = oxygen, white = hydrogen, grey = idealized bond). The space-fixed coordinate system is represented by XYZ , while the symmetry axis of the molecule is labeled by the molecule-fixed z -axis. The electronic orbital and spin angular momenta are represented by $\hat{\mathbf{L}}$ and $\hat{\mathbf{S}}$, respectively, and Λ and Σ are their projection along the symmetry axis of molecule. $\hat{\mathbf{R}}$ is the rotational angular momentum of the nuclei, $\hat{\mathbf{I}}$ is the nuclear spin angular momentum, and $\hat{\mathbf{J}}$ is the total angular momentum without the nuclear spin, $\hat{\mathbf{J}} = \hat{\mathbf{R}} + \hat{\mathbf{L}} + \hat{\mathbf{S}}$. The projection of $\hat{\mathbf{J}}$ along the space-fixed Z -axis is given by M_J , while the projection along the molecule-fixed z -axis is given by $\Omega = \Lambda + \Sigma$.

vibrational and electronic ground state of molecules by $v = 0$ and X , respectively, and to classify the molecular states with $^{2S+1}\Pi_{|\Lambda+\Sigma|}$ where Λ and Σ are the projections of the electronic orbital and spin angular momenta along the molecule-fixed z -axis, respectively, and Π stands for $|\Lambda| = 1$ [40, 42]. The effective Hamiltonian is given by [40, 8, 43, 9]

$$\hat{H}_0 = \hat{H}_{\text{SO}} + \hat{H}_{\text{MR}} + \hat{H}_{\text{SMR}} + \hat{H}_{\text{LD}} + \hat{H}_{\text{HF}} + \hat{H}_{\text{CD}}, \quad (27)$$

where \hat{H}_{SO} represents the spin-orbit coupling,

$$\hat{H}_{\text{SO}} = A_{\text{SO}} T_{q=0}^1(\hat{\mathbf{L}}) T_{q=0}^1(\hat{\mathbf{S}}), \quad (28)$$

\hat{H}_{MR} represents the rotational energy of the molecule,

$$\hat{H}_{\text{MR}} = B_N \hat{\mathbf{N}}^2, \quad (29)$$

\hat{H}_{SMR} is the spin-molecular rotation coupling,

$$\hat{H}_{\text{SMR}} = \gamma T^1(\hat{\mathbf{J}} - \hat{\mathbf{S}}) \cdot T^1(\hat{\mathbf{S}}), \quad (30)$$

\hat{H}_{LD} denotes the Λ -doubling terms,

$$\hat{H}_{\text{LD}} = \sum_{q=\pm 1} e^{-2iq\phi} \left[-Q T_{2q}^2(\hat{\mathbf{J}}, \hat{\mathbf{J}}) + (P + 2Q) T_{2q}^2(\hat{\mathbf{J}}, \hat{\mathbf{S}}) \right], \quad (31)$$

and \hat{H}_{HF} represents the hyperfine interactions,

$$\begin{aligned} \hat{H}_{\text{HF}} = & a T_{q=0}^1(\hat{\mathbf{I}}) T_{q=0}^1(\hat{\mathbf{L}}) + b_F T^1(\hat{\mathbf{I}}) \cdot T^1(\hat{\mathbf{S}}) + \sqrt{\frac{2}{3}} c T_{q=0}^2(\hat{\mathbf{I}}, \hat{\mathbf{S}}) + d \sum_{q=\pm 1} e^{-2iq\phi} T_{2q}^2(\hat{\mathbf{I}}, \hat{\mathbf{S}}) \\ & + c_I T^1(\hat{\mathbf{I}}) \cdot T^1(\hat{\mathbf{J}} - \hat{\mathbf{S}}) + c'_I \sum_{q=\pm 1} e^{-2iq\phi} \frac{1}{2} \left[T_{2q}^2(\hat{\mathbf{I}}, \hat{\mathbf{J}} - \hat{\mathbf{S}}) + T_{2q}^2(\hat{\mathbf{J}} - \hat{\mathbf{S}}, \hat{\mathbf{I}}) \right]. \end{aligned} \quad (32)$$

Table 1. Molecular parameters for OH in the $v = 0$ level of the $X^2\Pi$ ground state (in MHz) [9].

$A_{\text{so}} = -4168639.13(78)$
$B_N = 555660.97(11)$
$\gamma = -3574.88(49)$
$Q = -1159.991650$
$P = 7053.09846$
$a = 86.1116$
$b_F = -73.2537$
$c = 130.641$
$d = 56.6838$
$c_I = -0.09971$
$c'_I = 0.643 \times 10^{-2}$
$D = 57.1785(86)$
$H = 0.4236 \times 10^{-2}$
$\gamma_D = 0.7315$
$Q_D = 0.4420320$
$P_D = -1.550962$
$Q_H = -0.8237 \times 10^{-4}$
$P_H = 0.1647 \times 10^{-3}$
$d_D = -0.02276$

Finally, the centrifugal distortion corrections to the above terms are given by

$$\begin{aligned}
 \hat{H}_{\text{CD}} = & -D(\hat{\mathbf{N}}^2)^2 + H(\hat{\mathbf{N}}^2)^3 + \gamma_D \left\{ T^1(\hat{\mathbf{J}} - \hat{\mathbf{S}}) \cdot T^1(\hat{\mathbf{S}}) \right\} \hat{\mathbf{N}}^2 \\
 & + \sum_{q=\pm 1} e^{-2iq\phi} \left\{ -\frac{Q_D}{2} \left[T_{2q}^2(\hat{\mathbf{J}}, \hat{\mathbf{J}}) \hat{\mathbf{N}}^2 + \hat{\mathbf{N}}^2 T_{2q}^2(\hat{\mathbf{J}}, \hat{\mathbf{J}}) \right] + \frac{P_D + 2Q_D}{2} \left[T_{2q}^2(\hat{\mathbf{J}}, \hat{\mathbf{S}}) \hat{\mathbf{N}}^2 + \hat{\mathbf{N}}^2 T_{2q}^2(\hat{\mathbf{J}}, \hat{\mathbf{S}}) \right] \right\} \\
 & + \sum_{q=\pm 1} e^{-2iq\phi} \left\{ -\frac{Q_H}{2} \left[T_{2q}^2(\hat{\mathbf{J}}, \hat{\mathbf{J}}) (\hat{\mathbf{N}}^2)^2 + (\hat{\mathbf{N}}^2)^2 T_{2q}^2(\hat{\mathbf{J}}, \hat{\mathbf{J}}) \right] \right. \\
 & \quad \left. + \frac{P_H + 2Q_H}{2} \left[T_{2q}^2(\hat{\mathbf{J}}, \hat{\mathbf{S}}) (\hat{\mathbf{N}}^2)^2 + (\hat{\mathbf{N}}^2)^2 T_{2q}^2(\hat{\mathbf{J}}, \hat{\mathbf{S}}) \right] \right\} \\
 & + d_D \sum_{q=\pm 1} e^{-2iq\phi} \frac{1}{2} \left[T_{2q}^2(\hat{\mathbf{I}}, \hat{\mathbf{S}}) \hat{\mathbf{N}}^2 + \hat{\mathbf{N}}^2 T_{2q}^2(\hat{\mathbf{I}}, \hat{\mathbf{S}}) \right]. \tag{33}
 \end{aligned}$$

Note that these operators are written for calculation of their matrix elements with use of a Hund's case (a) basis in the molecule-fixed frame [40, 42], and that q denotes the component of the spherical tensor operator and ϕ is the azimuthal coordinate of the electronic orbit in the molecule-fixed frame. For the OH molecule, the Hund's case (a) basis consists of the simultaneous eigenstates of angular momenta, $\hat{\mathbf{L}}^2$, $\hat{\mathbf{S}}^2$, $\hat{\mathbf{J}}^2$ and $\hat{\mathbf{I}}^2$, projections on the molecule-fixed z -axis, \hat{L}_z , \hat{S}_z and \hat{J}_z , and projections on the space-fixed Z -axis, \hat{J}_Z and \hat{I}_Z , specified by $|L\Lambda, S\Sigma, J\Omega M_J, I M_I\rangle$ with $L = 1$, $\Lambda = \pm 1$, $S = 1/2$, $\Sigma = \pm 1/2$, $J \geq 1/2$, $\Omega = \Lambda + \Sigma$, $-J \leq M_J \leq J$, $I = 1/2$, and $M_I = \pm 1/2$. The matrix elements in the Hund's case (a) basis are given in Appendix B. Table 1 lists the values of molecular parameters of Eqs. (28)-(33), extracted from [9], and Figure 4 shows the energy scales of the effective Hamiltonian for

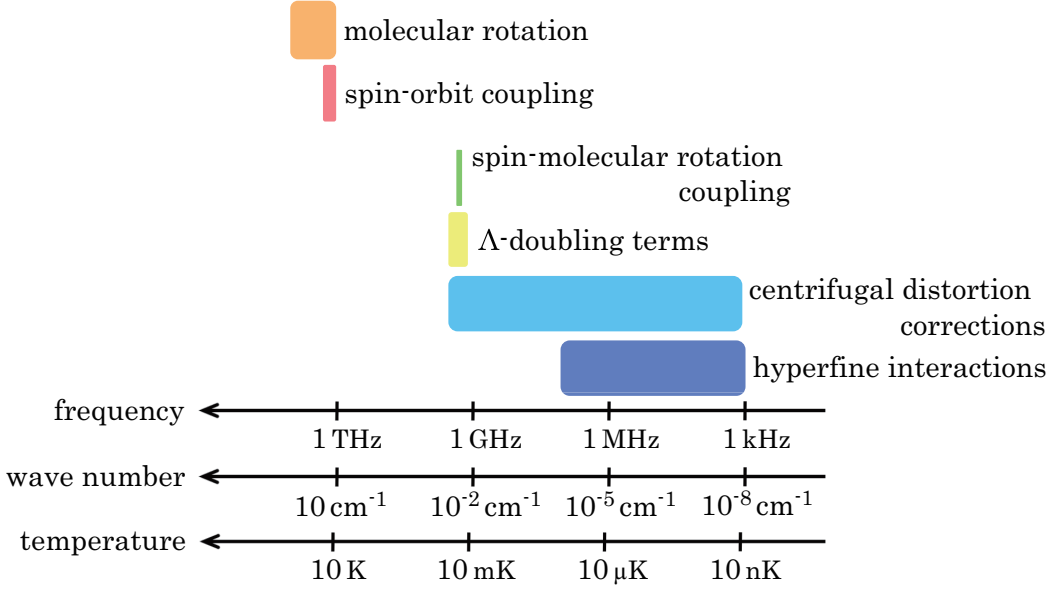


Figure 4. Energy scales of the effective Hamiltonian for OH in the $v = 0$ level of the $X^2\Pi$ ground state. Each energy scale is estimated by the size of matrix elements in the subspace of the lowest 96 states on a logarithmic scale. We consider frequency ν , wavenumber $1/\lambda$, and temperature T as units of energy by multiplying them through by the fundamental constants $h\nu$, hc/λ , and $k_B T$, respectively. These units of energy relate to each other: $1 \text{ MHz} \simeq 50 \mu\text{K} \simeq 3.3 \times 10^{-5} \text{ cm}^{-1}$.

OH. It is clear that one must take into account the centrifugal distortion corrections and the hyperfine interactions in order to obtain access to and investigate the physics of OH molecules at microKelvin temperatures and below.

3.2. The zero-field energy spectrum

We will investigate the energy spectrum of the Hamiltonian Eq. (27), focusing on the hyperfine structure of the lowest 16 states in the $^2\Pi_{3/2}$ manifold. Before going into details of the spectrum, let us overview the hierarchy of energy scales in the OH molecule. First of all, for the OH molecule the spin-orbit coupling gives the largest energy scale $A_{\text{so}} \sim -4 \text{ THz}$. Noting that the matrix elements of the spin-orbit coupling in Eq. (28) are diagonal in the Hund's case (a) basis and proportional to $\Lambda\Sigma$ (see Appendix B), the $^2\Pi$ states can be classified in two cases: one with $\Lambda\Sigma = 1/2$, and the other with $\Lambda\Sigma = -1/2$. The former case has the lower energy and it is also labeled by $|\Lambda + \Sigma| = 3/2$, called the $^2\Pi_{3/2}$ manifold, while the latter is labeled by $|\Lambda + \Sigma| = 1/2$, corresponding to the $^2\Pi_{1/2}$ manifold. The next largest energy scale is given by the rotational energy of molecule in Eq. (29) with $B_N \sim 0.5 \text{ THz}$. Since in the $^2\Pi_{3/2}$ manifold the molecular-axis projections Λ and Σ point in the same direction, the total angular momentum starts from $J = 3/2$ and increases by positive integers as the nuclei rotate faster. On the other hand, in the $^2\Pi_{1/2}$ manifold Λ and Σ point in opposite directions, and thus the total angular momentum can take the minimum, $J = 1/2$. Third, the spin-molecular rotation coupling in Eq. (30), where $\gamma \sim -3 \text{ GHz}$, becomes diagonal in our basis if we only consider the lowest 24 states consisting of $J = 3/2$ states in the $^2\Pi_{3/2}$ manifold and $J = 1/2$ states in the $^2\Pi_{1/2}$ manifold. However, there appear off-diagonal matrix elements that contribute when we take into account higher rotational states, and have to be folded in as corrections. Fourth, the Λ -doubling terms Eq. (31) with $Q \sim -1 \text{ GHz}$ and $P \sim 7 \text{ GHz}$ yield the Λ -doubling splittings in the spectrum, especially assigning 1 GHz splitting in

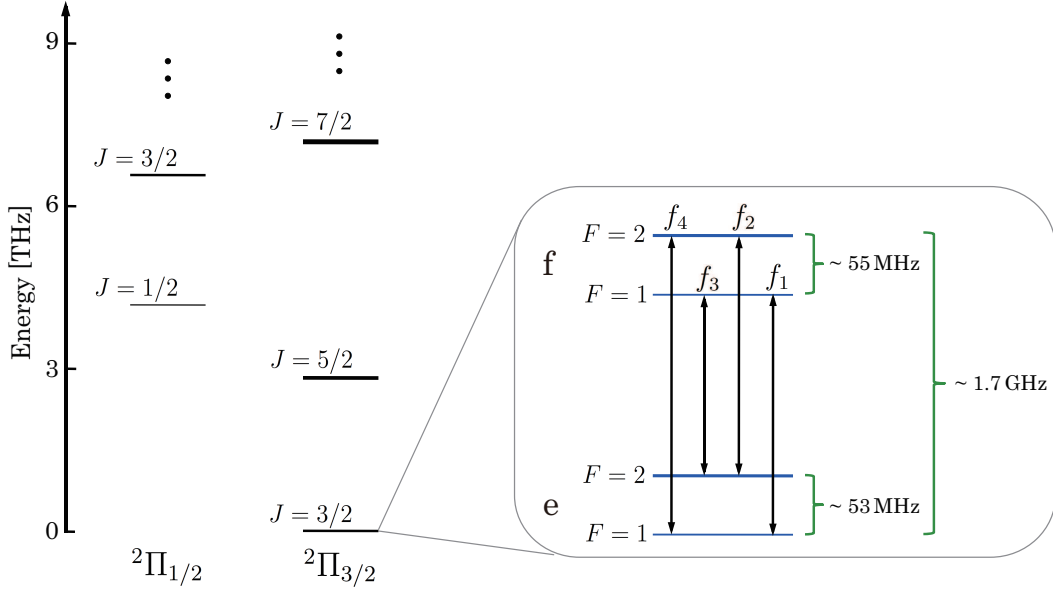


Figure 5. Zero-field energy spectrum and hyperfine structure of OH in the $v = 0$, $X^2\Pi_{3/2}$ ground state. Each rotational level, labeled by J , contains $4(2J + 1)$ states. A closeup of the hyperfine structure in $J = 3/2$ states of $^2\Pi_{3/2}$ shows the Λ -doubling splittings, represented by “e”-states for the negative parity states and “f”-states for the positive parity states, and also hyperfine splittings with transition frequencies f_1 , f_2 , f_3 , and f_4 .

the lowest $J = 3/2$ states of the $^2\Pi_{3/2}$ manifold. We remark that to obtain the Λ -doubling splittings in the $J = 3/2$ states of $^2\Pi_{3/2}$ we must include at least the $J = 3/2$ states of $^2\Pi_{1/2}$ in our model. Note also that the Λ -doubling terms hybridize fixed- Ω states, yielding the parity-conserved states in $^2\Pi_{3/2}$ as an appropriate basis in the absence of external fields,

$$|L, S; J, |\Omega|, M_J; I, M_I; \epsilon\rangle = \{ |L, |\Lambda\rangle |S, |\Sigma\rangle |J, |\Omega|, M_J\rangle |I, M_I\rangle + \epsilon(-1)^{J-S} |L, -|\Lambda\rangle |S, -|\Sigma\rangle |J, -|\Omega|, M_J\rangle |I, M_I\rangle \} / \sqrt{2}. \quad (34)$$

Here ϵ takes values of 1 and -1 corresponding to the positive and negative parity states, respectively. Finally, hyperfine interactions Eq. (32) and centrifugal distortion effects Eq. (33) give further microscopic structure in energy of tens of megahertz. As we will see later, the hyperfine interactions play a significant role in the emergence of level repulsions when we apply electric and magnetic fields.

We proceed to determine the energy spectrum of the Hamiltonian Eq. (27) numerically. Since we are interested in the spectrum of the lowest 16 states in the $^2\Pi_{3/2}$ manifold, we employed cutoffs for the unbounded quantum number J to consider a finite-dimensional subspace of states. More precisely, we restricted ourselves to states with $J = 1/2$ (8 states) and $J = 3/2$ (16 states) in the $^2\Pi_{1/2}$ manifold, and $J = 3/2$ (16 states), $J = 5/2$ (24 states), and $J = 7/2$ (32 states) in the $^2\Pi_{3/2}$ manifold, that is, the lowest 96 states as shown in Figure 5. Note that each rotational level labeled by J has further internal degrees of freedom, i.e., signs of Λ ($\Lambda = \pm|\Lambda|$), projections of $\hat{\mathbf{J}}$ ($M_J = 0, \pm 1, \dots, \pm J$), and projections of the nuclear spin ($M_I = \pm 1/2$), thus it contains $4(2J + 1)$ states. Figure 5 also shows a closeup of the hyperfine structure in $J = 3/2$ states of $^2\Pi_{3/2}$ where we described the Λ -doubling splittings by “e”-states for the negative parity states and “f”-states for the positive parity states, and hyperfine splittings with transition frequencies f_1 , f_2 , f_3 , and f_4 . We introduced the total angular momentum $\hat{\mathbf{F}} = \hat{\mathbf{J}} + \hat{\mathbf{I}}$ to label the hyperfine states. We numerically diagonalized the zero-field Hamiltonian Eq. (27) in the Hund’s case (a) basis consisted of the lowest 96 states, and calculated the energy spectrum of the lowest 16 states in the $^2\Pi_{3/2}$ manifold. Table 2 summarizes our numerical results along with experimental

Table 2. Hyperfine transition frequencies (in MHz) for OH in the $v = 0$, $X^2\Pi_{3/2}$ ground state.

	Calculated	Meulen <i>et al.</i> [3]	Hudson <i>et al.</i> [44]	Lev <i>et al.</i> [45]
f_1	1665.4006	1665.40184(10)	1665.401803(12)	—
f_2	1667.3576	1667.35903(10)	1667.358996(4)	—
f_3	1612.2300	1612.23101(20)	—	1612.230825(15)
f_4	1720.5282	1720.52998(10)	—	1720.529887(10)

data [3, 44, 45]. The largest deviation from the experimental data is in our calculation of f_4 , which determines an accuracy of calculations down to $1.8 \text{ kHz} \simeq 86 \text{ nK}$. From our results, we determine the energy of the Λ -doubling splittings to be $\Delta_{\text{LD}} = (f_1 + f_2 + f_3 + f_4)/4 = 1666.3791 \text{ MHz}$, and that of the hyperfine splitting for the even-parity states to be $\Delta_{\text{HF}}^{(e)} = (f_1 - f_3 + f_4 - f_2)/2 = 53.1706 \text{ MHz}$ and for the odd-parity states to be $\Delta_{\text{HF}}^{(f)} = (f_2 - f_3 + f_4 - f_1)/2 = 55.1276 \text{ MHz}$, respectively.

4. Hyperfine structure of OH molecule in combined electric and magnetic fields

In this section, we will add the Stark and Zeeman Hamiltonians to the zero-field Hamiltonian Eq. (27) in order to study the energy spectra under combined electric and magnetic fields. We first examine the Stark and Zeeman effects for the spectrum of $J = 3/2$ states in the $^2\Pi_{3/2}$ manifold separately, and then investigate the energy spectra in the presence of combined electric and magnetic fields.

4.1. The effective Hamiltonian of OH molecule in combined electric and magnetic fields

Let us consider the quantum rotor model for the OH molecule in the presence of combined electric and magnetic fields. Figure 6 shows a field configuration of electric and magnetic fields in which the magnetic field \mathbf{B} is chosen parallel to the space-fixed Z -axis, and the electric DC field \mathbf{E}_{DC} is in the space-fixed XZ -plane making an angle of θ_{BE} with the magnetic field. We also introduced Euler angles $\omega = (\phi, \theta, \chi)$ which define a general orientation of the molecule-fixed frame. The effective Hamiltonian of the OH molecule in the presence of combined electric and magnetic fields is then given by

$$\hat{H} = \hat{H}_0 + \hat{H}_S + \hat{H}_Z. \quad (35)$$

Here the zero-field Hamiltonian \hat{H}_0 is given in Eq. (27). The Stark Hamiltonian \hat{H}_S is given by

$$\hat{H}_S = -\hat{\mathbf{d}} \cdot \mathbf{E}_{\text{DC}}, \quad (36)$$

where $\hat{\mathbf{d}}$ is the electric dipole moment operator of OH, having a non-zero component along the molecule-fixed z -direction,

$$T_q^1(\hat{\mathbf{d}}) = \mu_z^{(e)} \delta_{q,0}, \quad (37)$$

with its permanent electric dipole moment $\mu_z^{(e)} = 1.65520(10) \text{ Debye}$ [46]. Noting that the angle between $\hat{\mathbf{d}}$ and \mathbf{E}_{DC} , θ_{dE} , satisfies $\cos \theta_{dE} = \cos \theta_{BE} \cos \theta + \sin \theta_{BE} \sin \theta \cos \phi$, we can rewrite the Stark Hamiltonian Eq. (36) as

$$\hat{H}_S = -\mu_z^{(e)} E_{\text{DC}} \sum_{p=0,\pm 1} d_{p,0}^{(1)}(\theta_{BE}) \mathcal{D}_{p,0}^{(1)*}(\omega), \quad (38)$$

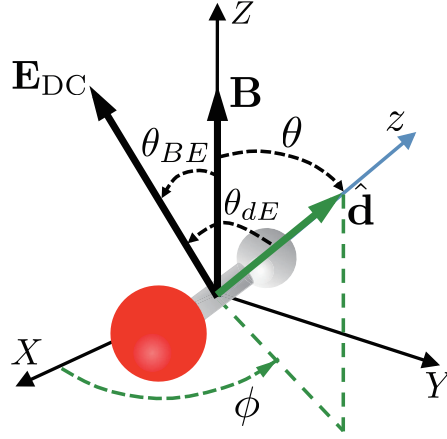


Figure 6. Field configuration and Euler angles defining a general orientation of the molecule-fixed axes. The magnetic field \mathbf{B} is chosen parallel to the space-fixed Z -axis, and the electric DC field \mathbf{E}_{DC} is in the space-fixed XZ -plane making an angle of θ_{BE} with the magnetic field. The electric dipole moment operator $\hat{\mathbf{d}}$ is parallel to the symmetry axis of molecule and θ_{dE} is the angle between $\hat{\mathbf{d}}$ and \mathbf{E}_{DC} . The Euler angles are labeled by $\omega = (\phi, \theta, \chi)$, though the angle χ is not shown here for simplicity.

Table 3. g -factors for OH in the $X^2\Pi$ state [8].

$g'_L = 1.00107(15)$
$g_S = 2.00152(36)$
$g_r = -0.633(19) \times 10^{-3}$
$g_\ell = 4.00(56) \times 10^{-3}$
$g'_\ell = 6.386(30) \times 10^{-3}$
$g_r^{e'} = 2.0446(23) \times 10^{-3}$

with the matrix elements of the Wigner D -matrix $\mathcal{D}_{p,q}^{(J)}$ and those of the reduced rotation matrix $d_{p,q}^{(1)}$ [40, 42]. In (35), the Zeeman Hamiltonian of the OH molecule is defined as

$$\begin{aligned}
 \hat{H}_Z = & g'_L \mu_B B_Z T_{p=0}^1(\hat{\mathbf{L}}) + g_S \mu_B B_Z T_{p=0}^1(\hat{\mathbf{S}}) - g_r \mu_B B_Z T_{p=0}^1(\hat{\mathbf{J}} - \hat{\mathbf{L}} - \hat{\mathbf{S}}) - g_N \mu_N B_Z T_{p=0}^1(\hat{\mathbf{I}}) \\
 & + g_l \mu_B B_Z \sum_{q=\pm 1} \mathcal{D}_{0,q}^{(1)*}(\omega) T_q^1(\hat{\mathbf{S}}) + g'_l \mu_B B_Z \sum_{q=\pm 1} e^{-2iq\phi} \mathcal{D}_{0,-q}^{(1)*}(\omega) T_q^1(\hat{\mathbf{S}}) \\
 & - g_r^{e'} \mu_B B_Z \sum_{q=\pm 1} \sum_{p=0,\pm 1} e^{-2iq\phi} (-1)^p \mathcal{D}_{-p,-q}^{(1)*}(\omega) T_p^1(\hat{\mathbf{J}} - \hat{\mathbf{S}}) \mathcal{D}_{0,-q}^{(1)*}(\omega), \quad (39)
 \end{aligned}$$

which contains, in order, the electronic orbital Zeeman effect, the electronic spin isotropic Zeeman effect, the rotational Zeeman effect, the nuclear spin Zeeman effect, and the electronic spin anisotropic Zeeman effect. Finally, the last two terms in Eq. (39) are parity-dependent and non-cylindrical Zeeman effects. The g -factors for OH in the $X^2\Pi$ state are listed in Table 3.

4.2. The Stark effect

We first examine how the Stark effect modifies the zero electric-field energy spectrum of OH in the absence of the magnetic field; $B_Z = 0$ and $\theta_{BE} = 0^\circ$. As in the calculation of the zero-field energy spectrum, we restricted ourselves to the lowest 96 states of OH, and diagonalize the Hamiltonian $\hat{H}_0 + \hat{H}_S$,

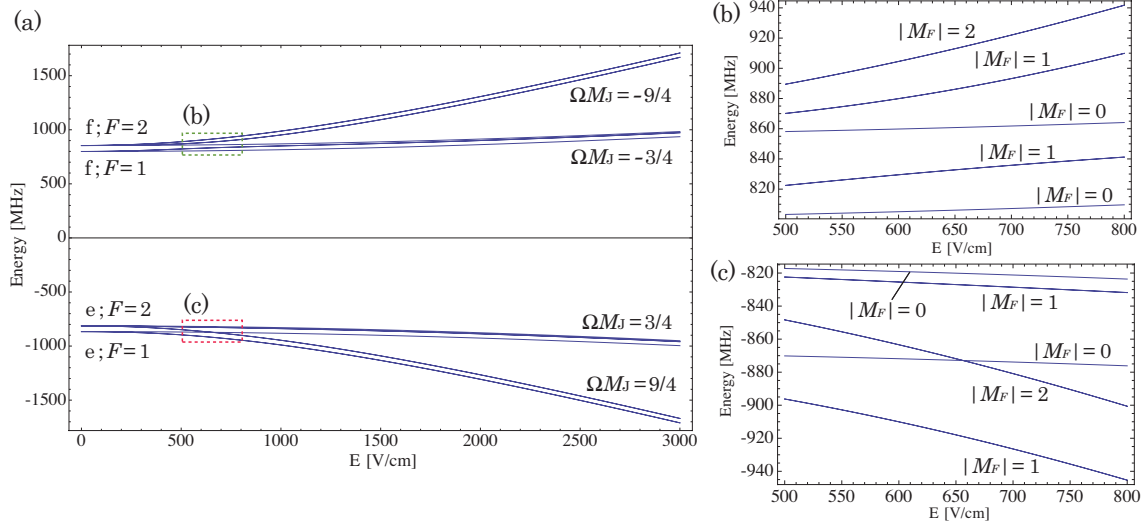


Figure 7. (a) The Stark effect of OH in the $v = 0$, $X^2\Pi_{3/2}$, $J = 3/2$ ground state, and the closeups of hyperfine structure: (b) for odd parity states (f-states) in zero field, and (c) for even parity states (e-states). There are always two-fold degeneracies with $M_F = \pm|M_F|$ except for $M_F = 0$ in the Stark spectrum.

given in Eqs. (27) and (38), to obtain the Stark effect of the $v = 0$, $X^2\Pi_{3/2}$, $J = 3/2$ ground state. Since in the electronic and vibrational ground states electric dipole moments of molecules depend only on their rotational structures, their matrix elements can be specified by quantum numbers J , Ω , and M_J in the Hund's case (a) basis,

$$\begin{aligned} & \langle L\Lambda', S\Sigma', J'\Omega' M_J', I M_I' | \hat{d}_Z | L\Lambda, S\Sigma, J\Omega M_J, I M_I \rangle \\ &= \mu_z^{(e)} \delta_{\Lambda, \Lambda'} \delta_{\Sigma, \Sigma'} \delta_{M_I, M_I'} (-1)^{M_J' - \Omega'} \sqrt{(2J' + 1)(2J + 1)} \begin{pmatrix} J' & 1 & J \\ -\Omega' & 0 & \Omega \end{pmatrix} \begin{pmatrix} J' & 1 & J \\ -M_J' & 0 & M_J \end{pmatrix}. \end{aligned} \quad (40)$$

Thus, the diagonal matrix elements of the Stark Hamiltonian \hat{H}_S with the electric field along the space-fixed Z -direction become

$$\langle L\Lambda, S\Sigma, J\Omega M_J, I M_I | \hat{H}_S | L\Lambda, S\Sigma, J\Omega M_J, I M_I \rangle = -\mu_z^{(e)} E_{DC} \frac{\Omega M_J}{J(J+1)}, \quad (41)$$

yielding a linear Stark effect, that is, a first order energy shift in the applied electric field. However, due to the Λ -doubling terms, the Hund's case (a) basis states are not the eigenstates of the zero-field Hamiltonian of OH. Instead, we can take the parity-conserved states Eq. (34) as an appropriate basis for zero or small applied fields. In this basis, the matrix elements become

$$\langle L, S, J | \Omega | M_J, I M_I; \epsilon' | \hat{H}_S | L, S, J | \Omega | M_J, I M_I; \epsilon \rangle = -\mu_z^{(e)} E_{DC} \frac{|\Omega| M_J}{J(J+1)} \left(\frac{1 - \epsilon\epsilon'}{2} \right), \quad (42)$$

showing that the diagonal matrix elements ($\epsilon = \epsilon'$) vanish and that the Stark shift is quadratic, i.e., second order in the applied electric field. This comes from the fact that the electric field is a vector field, a vector-valued function which is odd under spatial inversion, and thus the electric field mixes parity states [47, 11]. The structure of the matrix elements Eqs. (41) and (42) implies that states with different parities repel each other as the electric field is increased, and eventually form straight lines with opposite signs in their slopes. Figure 7 shows the Stark spectrum of OH in the $v = 0$, $X^2\Pi_{3/2}$, $J = 3/2$ ground state. Balancing one half of the Λ -doubling splitting Δ_{LD} with the linear Stark effect Eq. (41) averaged over $\Omega M_J = 3/4$ and $9/4$, we can estimate the critical value of the electric

field $E_c = 2499.84 \text{ V/cm} \sim 2.5 \text{ kV/cm}$, which determines whether the Stark effect becomes linear or quadratic at a given electric field. For weak electric fields $E_{\text{DC}} < E_c$, the zero-field Hamiltonian \hat{H}_0 dominates over the Stark term \hat{H}_S , and its perturbative effect based on the parity-conserved states gives quadratic curves as shown in Figure 7(a). On the other hand, for strong electric fields $E_{\text{DC}} > E_c$, the Stark term becomes dominant, and the energy spectrum is well approximated by the linear Stark effect Eq. (41). Figures 7(b) and (c) show the hyperfine structure in the presence of the electric field for states adiabatically connecting to odd and even parity states in zero field, respectively. Note that since the projection of the total angular momentum, M_F , is a good quantum number even in the presence of the electric field [47], there are always two-fold degeneracies with $M_F = \pm|M_F|$ except for $M_F = 0$.

4.3. The Zeeman effect

We proceed to consider the effect of non-zero static magnetic fields in the absence of the electric field; $E_{\text{DC}} = 0$. As before, we treat only the lowest 96 states of OH and diagonalize the Hamiltonian $\hat{H}_0 + \hat{H}_Z$, given in Eqs. (27) and (39), to study the Zeeman effect of the $v = 0$, $X^2\Pi_{3/2}$, $J = 3/2$ ground state. The Zeeman Hamiltonian of OH is dominated by contributions from the electronic orbital and spin isotropic Zeeman effects, as is seen from Table 3. In the Hund's case (a) basis, the diagonal matrix elements of these two operators can be written as

$$\begin{aligned} & \langle L\Lambda, S\Sigma, J\Omega M_J, IM_I | \{g'_L \mu_B B_Z T_{p=0}^1(\hat{\mathbf{L}}) + g_S \mu_B B_Z T_{p=0}^1(\hat{\mathbf{S}})\} | L\Lambda, S\Sigma, J\Omega M_J, IM_I \rangle \\ & = \mu_B B_Z (g'_L \Lambda + g_S \Sigma) \frac{\Omega M_J}{J(J+1)}, \end{aligned} \quad (43)$$

which become in the parity-conserved basis of the $^2\Pi_{3/2}$ states

$$\begin{aligned} & \langle L, S, J | \Omega | M_J, IM_I; \epsilon' | \{g'_L \mu_B B_Z T_{p=0}^1(\hat{\mathbf{L}}) + g_S \mu_B B_Z T_{p=0}^1(\hat{\mathbf{S}})\} | L, S, J | \Omega | M_J, IM_I; \epsilon \rangle \\ & = \mu_B B_Z (g'_L |\Lambda| + g_S |\Sigma|) \frac{|\Omega| M_J}{J(J+1)} \left(\frac{1 + \epsilon \epsilon'}{2} \right). \end{aligned} \quad (44)$$

Note here that the magnetic field is a pseudovector field, a vector-valued function which is even under spatial inversion, and therefore the magnetic field does not mix parity states while the electric field does [47, 11]. This can be seen in the matrix elements Eq. (44) which are diagonal in the parity-conserved basis. We illustrate this behavior in our Zeeman spectrum Figure 8(a) with closeups shown in Figures 8(b) and (c). The Zeeman spectrum of OH in the $v = 0$, $X^2\Pi_{3/2}$, $J = 3/2$ ground state is composed of two spectra with parity states opposite to each other. The Λ -doubling splitting separates these two spectra by Δ_{LD} , but except for such splitting they almost coincide with each other since the dominant part of the Zeeman effect Eq. (44) is the same for both the e- and f-states. Noting that M_F is a good quantum number in the absence of applied fields, we define a scale of the magnetic field that changes the good quantum number from M_F to M_J . We set the hyperfine splittings $\Delta_{\text{HF}}^{(e)}$ and $\Delta_{\text{HF}}^{(f)}$ equal to the linear Zeeman effect Eq. (44) averaged over $M_J = 1/2$ and $3/2$, and then obtain the critical values of the magnetic field; $B_c^{(e)} = 63.2576 \text{ G}$ for the e-states and $B_c^{(f)} = 65.5859 \text{ G}$ for the f-states. For strong magnetic fields $B_Z > B_c^{(e)}, B_c^{(f)}$, the Zeeman effect becomes dominant over the hyperfine structure in the zero-field, and the energy spectrum is well approximated by the linear Zeeman effect Eq. (44) in which each energy level can be specified by the quantum number M_J with hyperfine structure labeled

|| If we define the critical value of the electric field just by $\mu_z^{(e)} E_c = \Delta_{\text{LD}}/2$, we obtain $E_c = 999.935 \text{ V/cm} \sim 1 \text{ kV/cm}$ [11]. This definition is simpler than ours but seems inconsistent because it takes into account algebraic factors for the Λ -doubling splitting while not for the Stark effect.

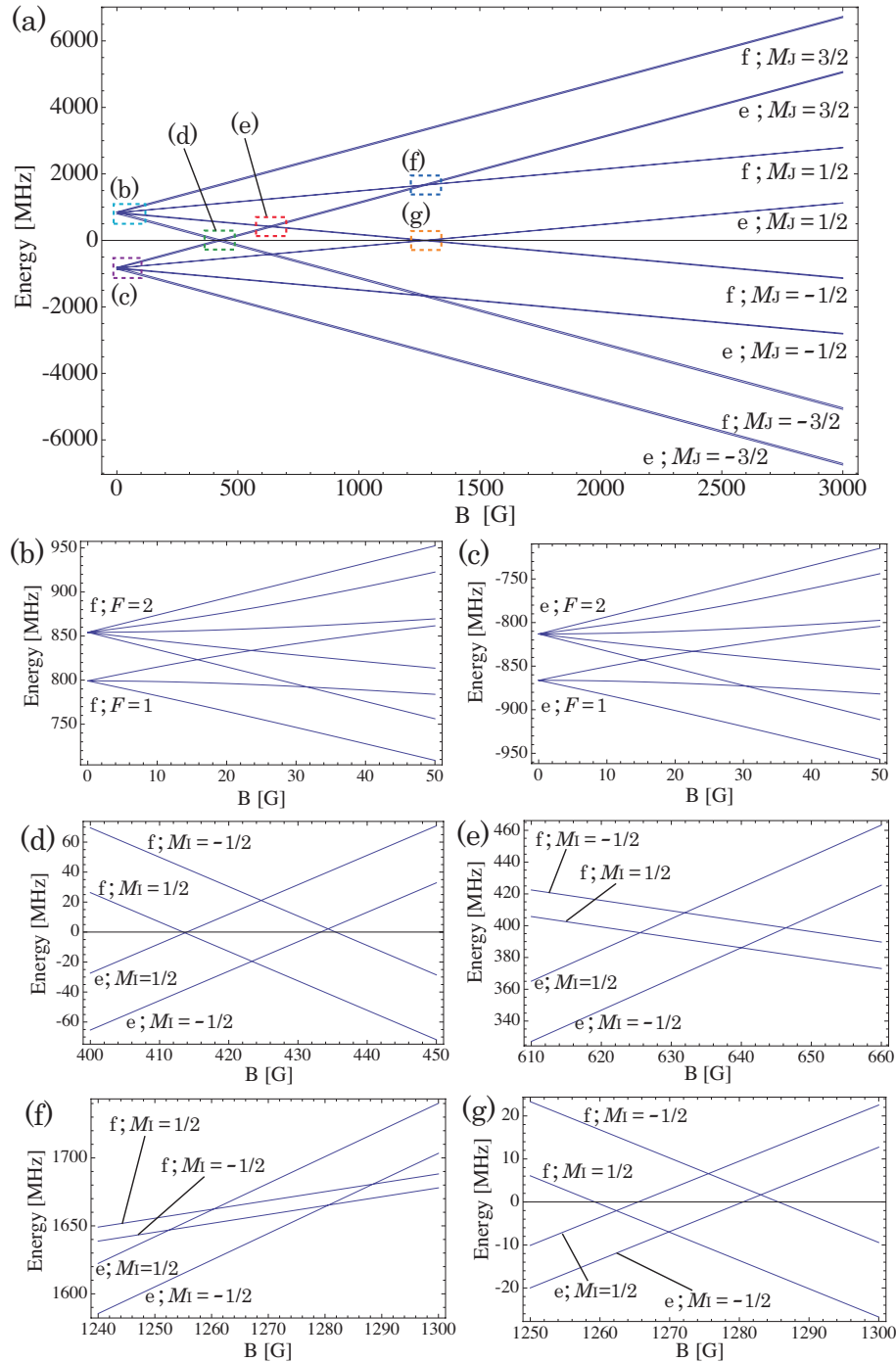


Figure 8. (a) The Zeeman effect for OH in the $v=0, X^2\Pi_{3/2}, J=3/2$ ground state. The closeups of hyperfine structure (b) for odd parity states (f-states) in zero field and (c) for even parity states (e-states) almost coincide with each other, except for the Λ -doubling splitting, since the dominant part of the Zeeman effect Eq.(44) is the same. (d)-(g) show the level crossings between opposite parity states $|e; M_I = \pm 1/2\rangle$ and $|f; M_I = \pm 1/2\rangle$, approaching to the asymptotic states (d) $|e; M_J = 3/2\rangle$ and $|f; M_J = -3/2\rangle$, (e) $|e; M_J = 3/2\rangle$ and $|f; M_J = -1/2\rangle$, (f) $|e; M_J = 3/2\rangle$ and $|f; M_J = 1/2\rangle$, and (g) $|e; M_J = 1/2\rangle$ and $|f; M_J = -1/2\rangle$, respectively.

by M_I , as shown in Figures 8(d)-(g). In contrast to the Stark spectrum Figure 7(a), the Λ -doubling splitting remains relevant over the whole range of the magnetic field.

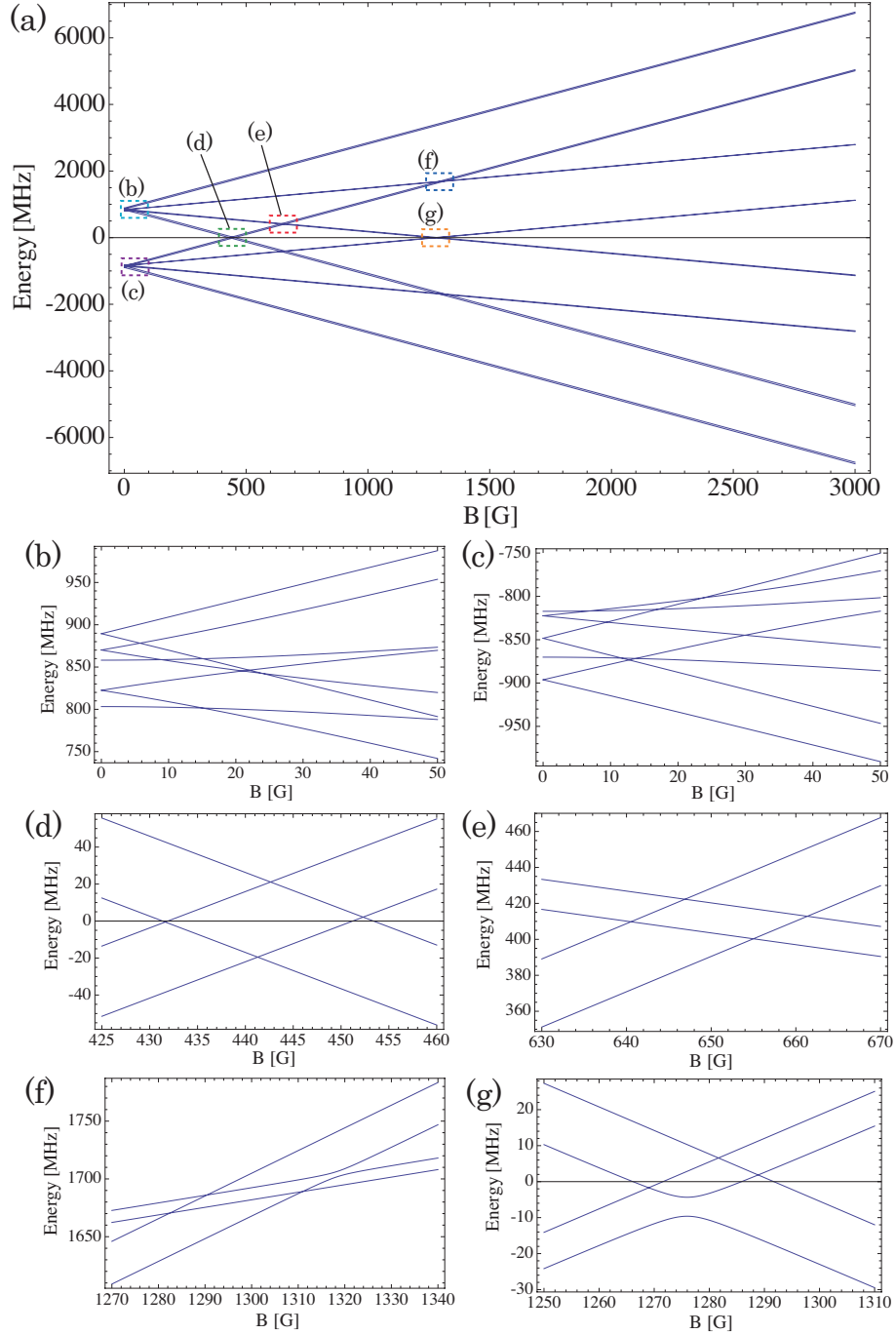


Figure 9. (a) The Zeeman effect for OH in the $v = 0$, $X^2\Pi_{3/2}$, $J = 3/2$ ground state, subject to a bias electric field with its strength $E_{DC} = 500$ V/cm and relative angle to the magnetic field $\theta_{BE} = 0^\circ$. (b) The closeups of hyperfine structure for odd parity states (f-states) in zero field and (c) for even parity states (e-states). (d)-(g) show the level crossings between opposite parity states $|e; M_I = \pm 1/2\rangle$ and $|f; M_I = \pm 1/2\rangle$, similar to Figures 8(d)-(g); however, here level repulsions also appear in (f) and (g) due to the Stark effect and hyperfine interactions.

4.4. Energy spectra in combined electric and magnetic fields

In the presence of both electric and magnetic fields, the energy spectrum of the OH molecule becomes more complicated since the Stark effect mixes parity states while the Zeeman effect does not. In addition, the hyperfine interactions Eq. (32) give rise to a new kind of level repulsion, which we call

Stark-induced hyperfine level repulsion.

We first fix the strength of the electric field E_{DC} and its angle θ_{BE} relative to the magnetic field, as shown in Figure 6. Then, we numerically diagonalize the effective Hamiltonian with external fields Eq. (35) and plot the energy spectrum of the lowest 16 states as a function of the applied magnetic field. Figure 9(a) shows the spectrum with the electric field parallel to the magnetic field, $\theta_{BE} = 0^\circ$ and strength $E_{\text{DC}} = 500$ V/cm. We observed that Figure 9(a) is quite similar to the pure Zeeman spectrum Figure 8(a). In this case, from the conservation of angular momentum, the matrix elements of the Stark term Eq. (36) becomes non-zero only between states with $\Delta J = 0, \pm 1$ and $\Delta M_J = 0$ (selection rule for $\theta_{BE} = 0^\circ$). On the other hand, states with different parities but same $M_J = 0$ are separated by the Λ -doubling splitting Δ_{LD} , and the magnetic field keeps them apart since the Zeeman effect Eq. (44) does not mix parity states. Therefore, one might consider that applying parallel electric and magnetic fields does not qualitatively change the pure Zeeman spectrum. However, looking at hyperfine structure, Figures 8(b)-(g) and Figures 9(b)-(g), we found that there are qualitative differences. In particular, the electric field causes level repulsions where both the Stark effects and hyperfine interactions play a significant role. First of all, the closeups Figures 9(b) and (c) differ from Figures 8(b) and (c), respectively, since the Stark effects break the hyperfine degeneracies in zero fields into the degeneracies with $M_F = \pm |M_F|$, as can be seen in Figures 7(b) and (c). Secondly, and even more intriguing, there are level repulsions in Figures 9(f) and (g), which do not appear in the pure Zeeman spectrum Figures 8(f) and (g). This is because under the electric field the energy eigenstates change from fixed-parity states into fixed- Ω states and such fixed- Ω fractions trigger level repulsions via hyperfine interactions. We remark that, due to the conservation of angular momentum, the hyperfine interactions have non-zero matrix elements between the same parity states with $\Delta M_J = -\Delta M_I$; this explains why only one of the four level crossings becomes level repulsion in Figures 9(f) and (g). These level repulsions in the Zeeman spectrum can be observed only when we take into account both Stark effect and hyperfine interactions, thus our appellation Stark-induced hyperfine level repulsions. There is no qualitative difference between Figures 8(d), (e) and Figures 9(d), (e) since the condition for the hyperfine interaction, $\Delta M_J = -\Delta M_I$, is not satisfied.

In the case of non-parallel electric and magnetic fields, $\theta_{BE} = 45^\circ$, the selection rule of the Stark term Eq. (36) for $\theta_{BE} = 45^\circ$ becomes $\Delta J = 0, \pm 1$ and $\Delta M_J = 0, \pm 1$, yielding level repulsions between different parity states with $\Delta M_J = \pm 1$ around $B \sim 1300$ G of Figure 10(a), where the strength of the electric field is set to be $E_{\text{DC}} = 500$ V/cm. These level repulsions, directly caused by the Stark effect, have energy gaps of 200-300 MHz and dominate over Stark-induced hyperfine level repulsions whose energy gaps are on the order of 10 MHz for $E_{\text{DC}} = 500$ V/cm. There are level repulsions also in Figures 10(b) and (c) satisfying the selection rule $\Delta M_J = \pm 1$, that do not appear in Figures 9(b) and (c) for $\theta_{BE} = 0^\circ$. The left- and right-most level repulsions in Figure 10(d) come from the Stark effect with $\Delta M_J = \pm 1$, while the left- and right-most level repulsions in Figure 10(e) from the Stark effect with $\Delta M_J = \pm 1$ and $\Delta M_J = 0$. We found another kind of level repulsion in Figures 10(d) and (e), see also Figures 10(f)-(i). The upper- and lower-most level repulsions in Figure 10 d) require not only the Stark effects with $\Delta M_J = \pm 1$ and $\Delta M_J = 0$ but also the hyperfine interactions; and the upper- and lower-most level repulsions in Figure 10(e) require the Stark effect with $\Delta M_J = \pm 1$ and the hyperfine interactions. As we will see next, some of these level repulsions become level *crossings* for $\theta_{BE} = 90^\circ$ since the Stark effect with $\Delta M_J = 0$ vanishes in that case.

When we apply an electric field perpendicular to the magnetic field, the selection rule of the Stark term Eq. (36) is $\Delta J = 0, \pm 1$ and $\Delta M_J = \pm 1$. Then, the Zeeman spectrum shown in Figure 11(a), where

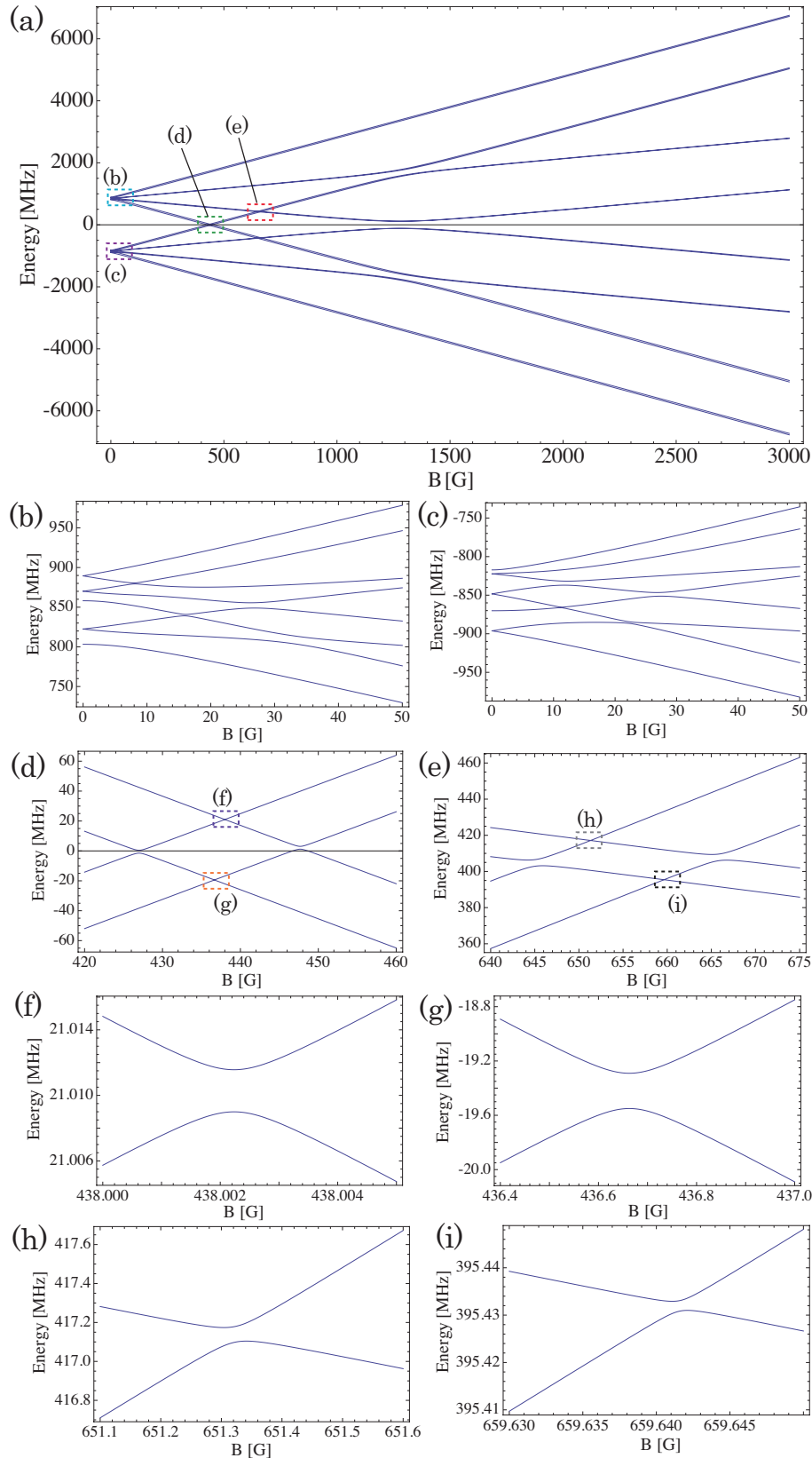


Figure 10. (a) The Zeeman effect for OH in the $v = 0$, $X^2\Pi_{3/2}$, $J = 3/2$ ground state, subject to a bias electric field with its strength $E_{DC} = 500$ V/cm and relative angle to the magnetic field $\theta_{BE} = 45^\circ$. (b) The closeups of hyperfine structure for odd parity states (f-states) in zero field and (c) for even parity states (e-states). (d) and (e) show the level repulsions between opposite parity states $|e; M_I = \pm 1/2\rangle$ and $|f; M_I = \pm 1/2\rangle$ approaching the asymptotic states (d) $|e; M_J = 3/2\rangle$ and $|f; M_J = -3/2\rangle$, and (e) $|e; M_J = 3/2\rangle$ and $|f; M_J = -1/2\rangle$, respectively. In contrast to Figures 8(d) and (e), all the crossings become avoided crossings, or level repulsions, in (d) and (e) as can be seen from (f)-(i) due to the field configuration allowing for transitions with $\Delta M_J = 0, \pm 1$.

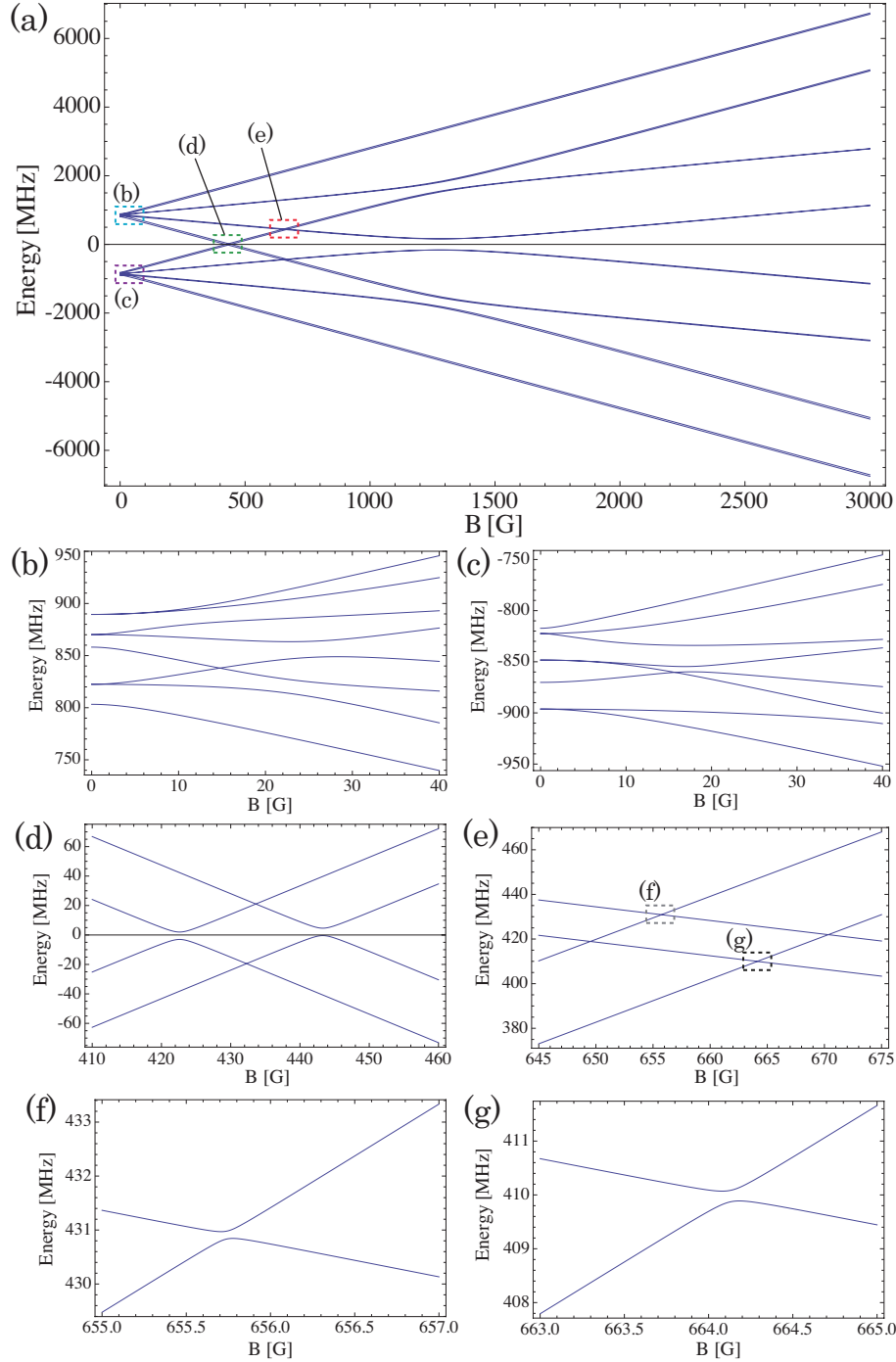


Figure 11. (a) The Zeeman effect for OH in the $v=0, X^2\Pi_{3/2}, J=3/2$ ground state, subject to a bias electric field with its strength $E_{DC} = 500$ V/cm and relative angle to the magnetic field $\theta_{BE} = 90^\circ$. (b) The closeups of hyperfine structure for odd parity states (f-states) in zero field and (c) for even parity states (e-states). (d) and (e) show the level repulsions between opposite parity states $|e; M_I = \pm 1/2\rangle$ and $|f; M_I = \pm 1/2\rangle$ as Figures 10(d) and (e), respectively, but the absence of a Stark effect with $\Delta M_J = 0$ changes the upper- and lower-most level repulsions in Figure 10(d) and the left- and right-most level repulsions in Figure 10(e) into level crossings. There are still level repulsions in (d) and (e) related to transitions with $\Delta M_J = \pm 1$, as seen in the further closeups (f) and (g).

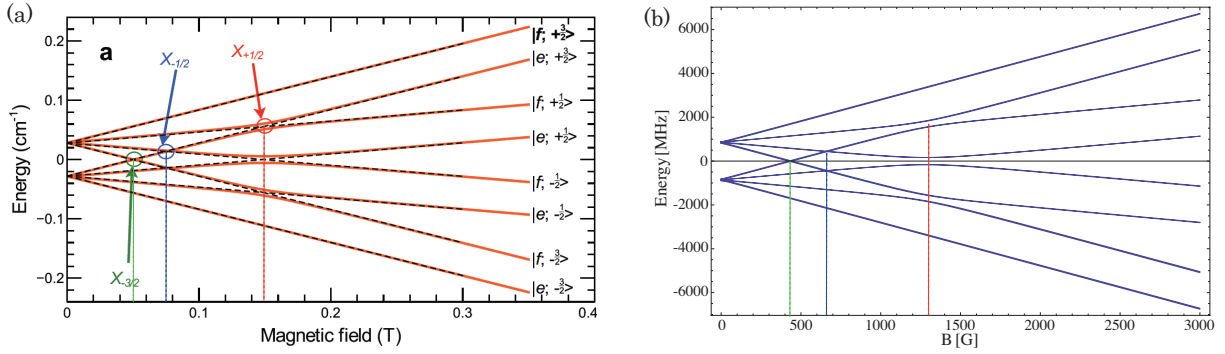


Figure 12. The Zeeman effect of OH in the $v = 0$, $X^2\Pi_{3/2}$, $J = 3/2$ ground state, subject to a bias electric field with its strength $E_{DC} = 500$ V/cm and relative angle to the magnetic field $\theta_{BE} = 90^\circ$. (a) is taken from Figure 1 in [7] where X_i labels the crossings of the $|e; 3/2\rangle$ state with the $|f; M_J = i\rangle$ states ($i = -3/2, -1/2, 1/2$), and (b) is our calculation, the same as Figure 11(a). We add vertical dashed lines to compare the values of the magnetic fields at the crossings.

$\theta_{BE} = 90^\circ$ and $E_{DC} = 500$ V/cm, has level repulsions between different parity states with $\Delta M_J = \pm 1$ around $B \sim 1300$ G as also seen in Figure 10(a). Also, Figures 11(b) and (c) are qualitatively the same as Figures 10(b) and (c), respectively, and their quantitative differences mainly result from differences in the transverse components of the electric field. The absence of a Stark effect with $\Delta M_J = 0$ changes some of the level repulsions into level crossings; the upper- and lower-most level repulsions in Figure 10(d) and the left- and right-most level repulsions in Figure 10(e) become level crossings, as seen in Figures 11(d) and (e).

4.5. Comparison with previous work

Finally, we shall compare our results with previous work on OH molecules. Recent works on the single-particle spectrum of OH in the presence of electric and/or magnetic fields dealt with phenomenological models which explicitly include the Lambda-doubling splitting Δ_{LD} and restrict themselves only to the lowest 16 states in the $^2\Pi_{3/2}$ manifold [11, 12, 7], or even to the lowest 8 states neglecting hyperfine structure [13, 14, 15, 16]. There exists one study which takes into account the effects of the higher rotational states and states in the $^2\Pi_{1/2}$ manifold [48], but still it neglects the hyperfine structure, centrifugal distortion effects, rotational Zeeman effect, electronic spin anisotropic Zeeman effect, and parity-dependent and non-cylindrical Zeeman effects. These effects are not negligible when we investigate cold and ultracold physics of OH molecules, as shown in Figure 4. As an illustration, we make a comparison of the OH spectrum between the result of [7] and ours. Figure 12 shows the Zeeman spectrum of OH in the presence of an electric field with strength $E_{DC} = 500$ V/cm and relative angle to the magnetic field $\theta_{BE} = 90^\circ$, where Figure 12(a) is taken from [7] and Figure 12(b) is our result. In Figure 12(a), X_i labels the crossings of the $|e; 3/2\rangle$ state with the $|f; M_J = i\rangle$ states ($i = -3/2, -1/2, 1/2$). We can see that the crossing $X_{-3/2}$ occurs around $B = 500$ G in Figure 12(a), while it occurs around $B = 430$ G in Figure 12(b). Also, the crossings $X_{-1/2}$ and $X_{1/2}$ occur around $B = 750$ G and $B = 1500$ G, respectively in Figure 12(a), while they occur around $B = 660$ G and $B = 1300$ G, respectively in Figure 12(b). The crossing points of X_i are reduced by more than 10 percent in our results since the states with $J = 3/2$ in the $^2\Pi_{1/2}$ manifold, which are not considered in the reduced model of [7], give non-negligible contributions via the electronic spin isotropic Zeeman coupling to the states with $J = 3/2$ in the $^2\Pi_{3/2}$ manifold.

5. Conclusions

We studied the single-particle energy spectra of the hydroxyl free radical OH in its lowest electronic and rovibrational level both in zero field and in combined electric and magnetic fields. The hyperfine interactions and centrifugal distortion effects are fully taken into account to yield the zero-field spectrum of the lowest ${}^2\Pi_{3/2}$ manifold to an accuracy of less than 2 kHz; in comparison, previous results obtained an accuracy of a few MHz. Our more precise calculations are necessary to enable accurate investigation of both the single-molecule and many-body physics of OH molecules at microKelvin temperatures and below, which we expect will be achieved in the near future. We also examined level crossings and repulsions in hyperfine structure caused by applied electric and magnetic fields. The level repulsions play a significant role in experiments allowing for transitions between low-field seeking and high-field seeking states. We found that in order to estimate the values of magnetic fields at the level repulsions in the ground states of the $J = 3/2$, ${}^2\Pi_{3/2}$ manifold it is necessary to include the coupling with the excited states of the $J = 3/2$, ${}^2\Pi_{1/2}$ manifold. In this paper, we dealt only with static electric and magnetic fields, leaving the microwave dressing of OH for future work. The microwave dressing via AC electric fields makes it possible to realize multi-component systems with both degeneracy and dipole-dipole interactions between different components, and thus explore a rapidly growing field, that is, quantum simulation of multi-component dipolar systems with ultracold molecules.

Acknowledgement

We thank Yehuda Band, Goulven Quémener, Jun Ye for helpful discussions. This research was supported in part by AFOSR Grant No. FA9550-11-1-0224 and by the NSF under Grants PHY-1207881 and NSF PHY11-25915. We appreciate the Aspen Center for Physics, supported in part by the NSF Grant No. 1066293, for hospitality during the writing of this paper.

Appendix A. Spherical tensor operators and related formulae

Let $\hat{\mathbf{A}}$, $\hat{\mathbf{B}}$ be arbitrary vector operators with their space-fixed components $(\hat{A}_X, \hat{A}_Y, \hat{A}_Z)$ and $(\hat{B}_X, \hat{B}_Y, \hat{B}_Z)$. Note that we use indices X, Y, Z for space-fixed components and x, y, z for molecule-fixed components of vector operators. We define ladder operators as usual, $\hat{A}_\pm = \hat{A}_X \pm i\hat{A}_Y$. Then the rank-1 (irreducible) spherical tensor operator $T^1(\hat{\mathbf{A}})$ is given by

$$T_0^1(\hat{\mathbf{A}}) = \hat{A}_Z, \quad T_1^1(\hat{\mathbf{A}}) = -\frac{1}{\sqrt{2}}\hat{A}_+, \quad T_{-1}^1(\hat{\mathbf{A}}) = \frac{1}{\sqrt{2}}\hat{A}_-. \quad (\text{A.1})$$

The scalar product of two rank-1 spherical tensor operators $T^1(\hat{\mathbf{A}})$ and $T^1(\hat{\mathbf{B}})$ becomes

$$T^1(\hat{\mathbf{A}}) \cdot T^1(\hat{\mathbf{B}}) = \sum_{p=0,\pm 1} (-1)^p T_p^1(\hat{\mathbf{A}}) T_{-p}^1(\hat{\mathbf{B}}) = \sum_{q=0,\pm 1} (-1)^q T_q^1(\hat{\mathbf{A}}) T_{-q}^1(\hat{\mathbf{B}}), \quad (\text{A.2})$$

where we specified space-fixed and molecule-fixed components by p and q , respectively. Also, the irreducible tensor product of two rank-1 spherical tensor operators $T^1(\hat{\mathbf{A}})$ and $T^1(\hat{\mathbf{B}})$ is given by

$$T_0^2(\hat{\mathbf{A}}, \hat{\mathbf{B}}) = \frac{1}{\sqrt{6}} \left[T_1^1(\hat{\mathbf{A}}) T_{-1}^1(\hat{\mathbf{B}}) + 2T_0^1(\hat{\mathbf{A}}) T_0^1(\hat{\mathbf{B}}) + T_{-1}^1(\hat{\mathbf{A}}) T_1^1(\hat{\mathbf{B}}) \right], \quad (\text{A.3})$$

$$T_{\pm 1}^2(\hat{\mathbf{A}}, \hat{\mathbf{B}}) = \frac{1}{\sqrt{2}} \left[T_{\pm 1}^1(\hat{\mathbf{A}}) T_0^1(\hat{\mathbf{B}}) + T_0^1(\hat{\mathbf{A}}) T_{\pm 1}^1(\hat{\mathbf{B}}) \right], \quad (\text{A.4})$$

$$T_{\pm 2}^2(\hat{\mathbf{A}}, \hat{\mathbf{B}}) = T_{\pm 1}^1(\hat{\mathbf{A}}) T_{\pm 1}^1(\hat{\mathbf{B}}). \quad (\text{A.5})$$

For a general definition of spherical tensor operators and their tensor products, see [40, 42]. A spherical tensor operator in the space-fixed frame, $T_p^1(\hat{\mathbf{A}})$, is related to its representation in the molecule-fixed frame, $T_q^1(\hat{\mathbf{A}})$, via the matrix elements of the Wigner D -matrix $\mathcal{D}_{p,q}^{(1)}$,

$$T_q^1(\hat{\mathbf{A}}) = \sum_{p=0,\pm 1} \mathcal{D}_{p,q}^{(1)}(\omega) T_p^1(\hat{\mathbf{A}}) , \quad (\text{A.6})$$

or equivalently,

$$T_p^1(\hat{\mathbf{A}}) = \sum_{q=0,\pm 1} \mathcal{D}_{p,q}^{(1)*}(\omega) T_q^1(\hat{\mathbf{A}}) . \quad (\text{A.7})$$

Here Euler angles $\omega = (\phi, \theta, \chi)$ define a general orientation of the molecule-fixed frame. In the following we will use the Wigner $3j$ -symbol, defined as

$$\begin{pmatrix} j_1 & j_2 & j_3 \\ m_1 & m_2 & m_3 \end{pmatrix} = (-1)^{j_1-j_2-m_3} (2j_3 + 1)^{-1/2} \langle j_1, m_1, j_2, m_2 | j_3, -m_3 \rangle , \quad (\text{A.8})$$

where $\langle j_1, m_1, j_2, m_2 | j_3, -m_3 \rangle$ is a Clebsch-Gordan coefficient. The Wigner-Eckart theorem gives the matrix elements of the spherical tensor operators,

$$\langle J', \Omega', M'_{J'} | T_p^1(\hat{\mathbf{J}}) | J, \Omega, M_J \rangle = \delta_{J,J'} \delta_{\Omega,\Omega'} (-1)^{J-M'_{J'}} \sqrt{J(J+1)(2J+1)} \begin{pmatrix} J & 1 & J \\ -M'_{J'} & p & M_J \end{pmatrix} , \quad (\text{A.9})$$

and

$$\begin{aligned} & \langle J', \Omega', M'_{J'} | T_p^2(\hat{\mathbf{J}}, \hat{\mathbf{J}}) | J, \Omega, M_J \rangle \\ &= \delta_{J,J'} \delta_{M_J, M'_{J'}} (-1)^{J-\Omega'} \frac{1}{2\sqrt{6}} \sqrt{(2J-1)2J(2J+1)(2J+2)(2J+3)} \begin{pmatrix} J & 2 & J \\ -\Omega' & p & \Omega \end{pmatrix} , \end{aligned} \quad (\text{A.10})$$

in the space-fixed frame, and

$$\langle J', \Omega', M'_{J'} | T_q^1(\hat{\mathbf{J}}) | J, \Omega, M_J \rangle = \delta_{J,J'} \delta_{M_J, M'_{J'}} (-1)^{J-\Omega'} \sqrt{J(J+1)(2J+1)} \begin{pmatrix} J & 1 & J \\ -\Omega' & q & \Omega \end{pmatrix} , \quad (\text{A.11})$$

in the molecule-fixed frame, where $|J, \Omega, M_J\rangle$ is the simultaneous eigenstate of operators $\hat{\mathbf{J}}^2$, \hat{J}_z , and \hat{J}_Z . Then, it is straightforward to have matrix elements of the nuclear spin operator and electronic spin operator,

$$\langle I, M'_I | T_p^1(\hat{\mathbf{I}}) | I, M_I \rangle = (-1)^{I-M'_I} \sqrt{I(I+1)(2I+1)} \begin{pmatrix} I & 1 & I \\ -M'_I & p & M_I \end{pmatrix} , \quad (\text{A.12})$$

and

$$\langle S, \Sigma' | T_q^1(\hat{\mathbf{S}}) | S, \Sigma \rangle = (-1)^{S-\Sigma'} \sqrt{S(S+1)(2S+1)} \begin{pmatrix} S & 1 & S \\ -\Sigma' & q & \Sigma \end{pmatrix} , \quad (\text{A.13})$$

where $|I, M_I\rangle$ and $|S, \Sigma\rangle$ are the simultaneous eigenstates of operators $\hat{\mathbf{I}}^2$, \hat{I}_Z and $\hat{\mathbf{S}}^2$, \hat{S}_z , respectively. We need a few more formulae to calculate the matrix elements of the effective Hamiltonian for OH molecule,

$$\begin{aligned} & \langle J', \Omega', M'_{J'} | \mathcal{D}_{p,q}^{(1)*}(\omega) | J, \Omega, M_J \rangle \\ &= (-1)^{M'_{J'}-\Omega'} \sqrt{(2J'+1)(2J+1)} \begin{pmatrix} J' & 1 & J \\ -\Omega' & q & \Omega \end{pmatrix} \begin{pmatrix} J' & 1 & J \\ -M'_{J'} & p & M_J \end{pmatrix} , \end{aligned} \quad (\text{A.14})$$

and

$$\begin{aligned} \langle J', \Omega', M'_{J'} | \sum_{p=0, \pm 1} (-1)^p T_p^1(\hat{\mathbf{J}}) \mathcal{D}_{-p, q}^{(1)*}(\omega) | J, \Omega, M_J \rangle \\ = \delta_{J, J'} \delta_{M_J, M'_{J'}} (-1)^{J-\Omega'} \sqrt{J(J+1)(2J+1)} \begin{pmatrix} J & 1 & J \\ -\Omega' & q & \Omega \end{pmatrix}. \end{aligned} \quad (\text{A.15})$$

We finally remark that due to the anomalous commutation relation in the molecule-fixed frame,

$$[\hat{J}_\alpha, \hat{J}_\beta] = -i \epsilon_{\alpha\beta\gamma} \hat{J}_\gamma \quad (\alpha, \beta, \gamma \in \{x, y, z\}), \quad (\text{A.16})$$

we should replace the the molecule-fixed components of spherical tensor operators as $T_q^1(\hat{\mathbf{J}}) \rightarrow (-1)^q T_{-q}^1(\hat{\mathbf{J}})$ before calculating matrix elements. A detailed derivation of the above formulae may be found in [40, 42].

Appendix B. Matrix elements of the effective Hamiltonian

We have chosen a Hund's case (a) basis in the molecule-fixed frame to obtain a representation of the molecular Hamiltonian,

$$|L\Lambda, S\Sigma, J\Omega M_J, I M_I\rangle = |L, \Lambda\rangle |S, \Sigma\rangle |J, \Omega, M_J\rangle |I, M_I\rangle \quad (\text{B.1})$$

with quantum numbers $L = 1$, $\Lambda = \pm 1$, $S = 1/2$, $\Sigma = \pm 1/2$, $J \geq 1/2$, $\Omega = \Lambda + \Sigma$, $-J \leq M_J \leq J$, $I = 1/2$, and $M_I = \pm 1/2$. Based on the formulae given in Appendix A, we can derive the following 23 matrix elements of the effective Hamiltonian for OH.

(1) Spin-orbit coupling

$$\begin{aligned} \langle L\Lambda', S\Sigma', J'\Omega' M'_{J'}, I M'_I | A_{\text{so}} T_{q=0}^1(\hat{\mathbf{L}}) T_{q=0}^1(\hat{\mathbf{S}}) | L\Lambda, S\Sigma, J\Omega M_J, I M_I \rangle \\ = A_{\text{so}} \Lambda \Sigma \delta_{\Lambda, \Lambda'} \delta_{\Sigma, \Sigma'} \delta_{J, J'} \delta_{\Omega, \Omega'} \delta_{M_J, M'_{J'}} \delta_{M_I, M'_I}. \end{aligned} \quad (\text{B.2})$$

(2) Molecular rotation

$$\begin{aligned} \langle L\Lambda', S\Sigma', J'\Omega' M'_{J'}, I M'_I | B_N \hat{\mathbf{N}}^2 | L\Lambda, S\Sigma, J\Omega M_J, I M_I \rangle \\ = B_N [J(J+1) + S(S+1) - 2\Omega\Sigma] \delta_{\Lambda, \Lambda'} \delta_{\Sigma, \Sigma'} \delta_{J, J'} \delta_{\Omega, \Omega'} \delta_{M_J, M'_{J'}} \delta_{M_I, M'_I} \\ - 2B_N \delta_{\Lambda, \Lambda'} \delta_{J, J'} \delta_{M_J, M'_{J'}} \delta_{M_I, M'_I} \\ \times (-1)^{J-\Omega'+S-\Sigma'} \sqrt{J(J+1)(2J+1)S(S+1)(2S+1)} \sum_{q=\pm 1} \begin{pmatrix} J & 1 & J \\ -\Omega' & q & \Omega \end{pmatrix} \begin{pmatrix} S & 1 & S \\ -\Sigma' & q & \Sigma \end{pmatrix}. \end{aligned} \quad (\text{B.3})$$

(3) Spin-molecular rotation coupling

$$\begin{aligned} \langle L\Lambda', S\Sigma', J'\Omega' M'_{J'}, I M'_I | \gamma T^1(\hat{\mathbf{J}} - \hat{\mathbf{S}}) \cdot T^1(\hat{\mathbf{S}}) | L\Lambda, S\Sigma, J\Omega M_J, I M_I \rangle \\ = \gamma [\Omega\Sigma - S(S+1)] \delta_{\Lambda, \Lambda'} \delta_{\Sigma, \Sigma'} \delta_{J, J'} \delta_{\Omega, \Omega'} \delta_{M_J, M'_{J'}} \delta_{M_I, M'_I} \\ + \gamma \delta_{\Lambda, \Lambda'} \delta_{J, J'} \delta_{M_J, M'_{J'}} \delta_{M_I, M'_I} \\ \times (-1)^{J-\Omega'+S-\Sigma'} \sqrt{J(J+1)(2J+1)S(S+1)(2S+1)} \sum_{q=\pm 1} \begin{pmatrix} J & 1 & J \\ -\Omega' & q & \Omega \end{pmatrix} \begin{pmatrix} S & 1 & S \\ -\Sigma' & q & \Sigma \end{pmatrix}. \end{aligned} \quad (\text{B.4})$$

(4) Λ -doubling term

$$\begin{aligned} \langle L\Lambda', S\Sigma', J'\Omega' M'_{J'}, I M'_I | \sum_{q=\pm 1} e^{-2iq\phi} \left[-Q T_{2q}^2(\hat{\mathbf{J}}, \hat{\mathbf{J}}) + (P + 2Q) T_{2q}^2(\hat{\mathbf{J}}, \hat{\mathbf{S}}) \right] | L\Lambda, S\Sigma, J\Omega M_J, I M_I \rangle \\ = \delta_{J, J'} \delta_{M_J, M'_{J'}} \delta_{M_I, M'_I} (-1)^{J-\Omega'} \sqrt{J(2J+1)} \sum_{q=\pm 1} \delta_{\Lambda', \Lambda-2q} \end{aligned}$$

$$\begin{aligned} & \times \left\{ \frac{Q}{2\sqrt{3}} \delta_{\Sigma, \Sigma'} \sqrt{(2J-1)(2J+2)(2J+3)} \begin{pmatrix} J & 2 & J \\ -\Omega' & -2q & \Omega \end{pmatrix} \right. \\ & \left. + (P+2Q)(-1)^{S-\Sigma'} \sqrt{(J+1)S(S+1)(2S+1)} \begin{pmatrix} J & 1 & J \\ -\Omega' & -q & \Omega \end{pmatrix} \begin{pmatrix} S & 1 & S \\ -\Sigma' & q & \Sigma \end{pmatrix} \right\}. \end{aligned} \quad (\text{B.5})$$

(5) Magnetic hyperfine interaction (I)

$$\begin{aligned} & \langle L\Lambda', S\Sigma', J'\Omega' M'_{J'}, I M'_I | a T_{q=0}^1(\hat{\mathbf{I}}) T_{q=0}^1(\hat{\mathbf{L}}) | L\Lambda, S\Sigma, J\Omega M_J, I M_I \rangle \\ & = a\Lambda \delta_{\Lambda, \Lambda'} \delta_{\Sigma, \Sigma'} (-1)^{M'_{J'} - \Omega' + I - M'_I} \sqrt{I(I+1)(2I+1)(2J'+1)(2J+1)} \begin{pmatrix} J' & 1 & J \\ -\Omega' & 0 & \Omega \end{pmatrix} \\ & \times \sum_{p=0, \pm 1} (-1)^p \begin{pmatrix} J' & 1 & J \\ -M'_{J'} & p & M_J \end{pmatrix} \begin{pmatrix} I & 1 & I \\ -M'_I & -p & M_I \end{pmatrix}. \end{aligned} \quad (\text{B.6})$$

(6) Magnetic hyperfine interaction (II)

$$\begin{aligned} & \langle L\Lambda', S\Sigma', J'\Omega' M'_{J'}, I M'_I | b_F T^1(\hat{\mathbf{I}}) \cdot T^1(\hat{\mathbf{S}}) | L\Lambda, S\Sigma, J\Omega M_J, I M_I \rangle \\ & = b_F \delta_{\Lambda, \Lambda'} (-1)^{M'_{J'} - \Omega' + I - M'_I + S - \Sigma'} \sqrt{(2J'+1)(2J+1)I(I+1)(2I+1)S(S+1)(2S+1)} \\ & \times \sum_{p, q=0, \pm 1} (-1)^p \begin{pmatrix} J' & 1 & J \\ -\Omega' & q & \Omega \end{pmatrix} \begin{pmatrix} J' & 1 & J \\ -M'_{J'} & p & M_J \end{pmatrix} \begin{pmatrix} I & 1 & I \\ -M'_I & -p & M_I \end{pmatrix} \begin{pmatrix} S & 1 & S \\ -\Sigma' & q & \Sigma \end{pmatrix}. \end{aligned} \quad (\text{B.7})$$

(7) Magnetic hyperfine interaction (III)

$$\begin{aligned} & \langle L\Lambda', S\Sigma', J'\Omega' M'_{J'}, I M'_I | \left\{ \sqrt{\frac{2}{3}} c T_{q=0}^2(\hat{\mathbf{I}}, \hat{\mathbf{S}}) + d \sum_{q=\pm 1} e^{-2iq\phi} T_{2q}^2(\hat{\mathbf{I}}, \hat{\mathbf{S}}) \right\} | L\Lambda, S\Sigma, J\Omega M_J, I M_I \rangle \\ & = (-1)^{M'_{J'} - \Omega' + I - M'_I + S - \Sigma'} \sqrt{(2J'+1)(2J+1)I(I+1)(2I+1)S(S+1)(2S+1)} \\ & \times \sum_{p=0, \pm 1} (-1)^p \begin{pmatrix} J' & 1 & J \\ -M'_{J'} & p & M_J \end{pmatrix} \begin{pmatrix} I & 1 & I \\ -M'_I & -p & M_I \end{pmatrix} \\ & \times \left\{ \sqrt{\frac{10}{3}} c \delta_{\Lambda, \Lambda'} \sum_{q_1=0, \pm 1} (-1)^{q_1} \begin{pmatrix} 1 & 2 & 1 \\ -q_1 & 0 & q_1 \end{pmatrix} \begin{pmatrix} J' & 1 & J \\ -\Omega' & q_1 & \Omega \end{pmatrix} \begin{pmatrix} S & 1 & S \\ -\Sigma' & q_1 & \Sigma \end{pmatrix} \right. \\ & \left. + d \sum_{q=\pm 1} \delta_{\Lambda', \Lambda-2q} \begin{pmatrix} J' & 1 & J \\ -\Omega' & -q & \Omega \end{pmatrix} \begin{pmatrix} S & 1 & S \\ -\Sigma' & q & \Sigma \end{pmatrix} \right\}. \end{aligned} \quad (\text{B.8})$$

(8) Magnetic hyperfine interaction (IV)

$$\begin{aligned} & \langle L\Lambda', S\Sigma', J'\Omega' M'_{J'}, I M'_I | c_I T^1(\hat{\mathbf{I}}) \cdot T^1(\hat{\mathbf{J}} - \hat{\mathbf{S}}) | L\Lambda, S\Sigma, J\Omega M_J, I M_I \rangle \\ & = c_I \delta_{\Lambda, \Lambda'} (-1)^{I - M'_I} \sqrt{I(I+1)(2I+1)} \sum_{p=0, \pm 1} (-1)^p \begin{pmatrix} J' & 1 & J \\ -M'_{J'} & p & M_J \end{pmatrix} \begin{pmatrix} I & 1 & I \\ -M'_I & -p & M_I \end{pmatrix} \\ & \times \left\{ \delta_{\Sigma, \Sigma'} \delta_{J, J'} \delta_{\Omega, \Omega'} (-1)^{J - M'_{J'}} \sqrt{J(J+1)(2J+1)} \right. \\ & \left. - (-1)^{M'_{J'} - \Omega' + S - \Sigma'} \sqrt{(2J'+1)(2J+1)S(S+1)(2S+1)} \sum_{q=0, \pm 1} \begin{pmatrix} J' & 1 & J \\ -\Omega' & q & \Omega \end{pmatrix} \begin{pmatrix} S & 1 & S \\ -\Sigma' & q & \Sigma \end{pmatrix} \right\}. \end{aligned} \quad (\text{B.9})$$

(9) Magnetic hyperfine interaction (V)

$$\begin{aligned} & \langle L\Lambda', S\Sigma', J'\Omega' M'_{J'}, I M'_I | c'_I \sum_{q=\pm 1} e^{-2iq\phi} \frac{1}{2} \left[T_{2q}^2(\hat{\mathbf{I}}, \hat{\mathbf{J}} - \hat{\mathbf{S}}) + T_{2q}^2(\hat{\mathbf{J}} - \hat{\mathbf{S}}, \hat{\mathbf{I}}) \right] | L\Lambda, S\Sigma, J\Omega M_J, I M_I \rangle \\ & = -\frac{c'_I}{2} (-1)^{I - M'_I} \sqrt{I(I+1)(2I+1)(2J'+1)(2J+1)} \sum_{p=0, \pm 1} (-1)^p \begin{pmatrix} I & 1 & I \\ -M'_I & -p & M_I \end{pmatrix} \begin{pmatrix} J' & 1 & J \\ -M'_{J'} & p & M_J \end{pmatrix} \end{aligned} \quad (\text{B.10})$$

$$\begin{aligned}
& \times \sum_{q=\pm 1} \delta_{\Lambda', \Lambda-2q} \left\{ 2(-1)^{S-\Sigma'+M'_{J'}-\Omega'} \sqrt{S(S+1)(2S+1)} \begin{pmatrix} S & 1 & S \\ -\Sigma' & q & \Sigma \end{pmatrix} \begin{pmatrix} J' & 1 & J \\ -\Omega' & -q & \Omega \end{pmatrix} \right. \\
& + \delta_{\Sigma, \Sigma'} \theta(3/2 - |\Omega' + q|) (-1)^{J+M'_{J'}} \sqrt{J(J+1)(2J+1)} \begin{pmatrix} J' & 1 & J \\ -\Omega' & -q & \Omega' + q \end{pmatrix} \begin{pmatrix} J & 1 & J \\ -\Omega' - q & -q & \Omega \end{pmatrix} \\
& \left. + \delta_{\Sigma, \Sigma'} \theta(3/2 - |\Omega' + q|) (-1)^{J'+M'_{J'}} \sqrt{J'(J'+1)(2J'+1)} \begin{pmatrix} J' & 1 & J' \\ -\Omega' & -q & \Omega' + q \end{pmatrix} \begin{pmatrix} J' & 1 & J' \\ -\Omega' - q & -q & \Omega \end{pmatrix} \right\}.
\end{aligned}$$

(10) Centrifugal distortion effect to molecular rotation (I)

$$\begin{aligned}
& - \langle L\Lambda', S\Sigma', J'\Omega' M'_{J'}, I M'_I | D(\hat{\mathbf{N}}^2)^2 | L\Lambda, S\Sigma, J\Omega M_J, I M_I \rangle \\
& = -D \delta_{\Lambda, \Lambda'} \delta_{J, J'} \delta_{M_J, M'_{J'}} \delta_{M_I, M'_I} \\
& \times \left\{ \delta_{\Omega, \Omega'} \delta_{\Sigma, \Sigma'} [J(J+1) + S(S+1) - 2\Omega\Sigma]^2 \right. \\
& \quad - 2(-1)^{J-\Omega'+S-\Sigma'} \sqrt{J(J+1)(2J+1)S(S+1)(2S+1)} \\
& \quad \times [2J(J+1) + 2S(S+1) - 2\Omega'\Sigma' - 2\Omega\Sigma] \sum_{q=\pm 1} \begin{pmatrix} J & 1 & J \\ -\Omega' & q & \Omega \end{pmatrix} \begin{pmatrix} S & 1 & S \\ -\Sigma' & q & \Sigma \end{pmatrix} \\
& \quad \left. + 4\delta_{\Omega, \Omega'} \delta_{\Sigma, \Sigma'} J(J+1)(2J+1)S(S+1)(2S+1) \right. \\
& \quad \left. \times \sum_{q=\pm 1} \left[\begin{pmatrix} J & 1 & J \\ -\Omega & q & \Omega - q \end{pmatrix} \begin{pmatrix} S & 1 & S \\ -\Sigma & q & \Sigma - q \end{pmatrix} \right]^2 \theta(3/2 - |\Omega - q|) \right\}. \tag{B.11}
\end{aligned}$$

(11) Centrifugal distortion effect to molecular rotation (II)

$$\begin{aligned}
& \langle L\Lambda', S\Sigma', J'\Omega' M'_{J'}, I M'_I | H(\hat{\mathbf{N}}^2)^3 | L\Lambda, S\Sigma, J\Omega M_J, I M_I \rangle \\
& = H \delta_{\Lambda, \Lambda'} \delta_{J, J'} \delta_{M_J, M'_{J'}} \delta_{M_I, M'_I} \\
& \times \left\{ \delta_{\Omega, \Omega'} \delta_{\Sigma, \Sigma'} [J(J+1) + S(S+1) - 2\Omega\Sigma]^3 \right. \\
& \quad + 4\delta_{\Omega, \Omega'} \delta_{\Sigma, \Sigma'} J(J+1)(2J+1)S(S+1)(2S+1) \sum_{q=\pm 1} \theta(3/2 - |\Omega - q|) \\
& \quad \times [3J(J+1) + 3S(S+1) - 4\Omega\Sigma - 2(\Omega - q)(\Sigma - q)] \left[\begin{pmatrix} J & 1 & J \\ -\Omega & q & \Omega - q \end{pmatrix} \begin{pmatrix} S & 1 & S \\ -\Sigma & q & \Sigma - q \end{pmatrix} \right]^2 \\
& \quad - 2(-1)^{J-\Omega'+S-\Sigma'} \sqrt{J(J+1)(2J+1)S(S+1)(2S+1)} \sum_{q=\pm 1} \begin{pmatrix} J & 1 & J \\ -\Omega' & q & \Omega \end{pmatrix} \begin{pmatrix} S & 1 & S \\ -\Sigma' & q & \Sigma \end{pmatrix} \\
& \quad \times \left[[J(J+1) + S(S+1) - 2\Omega'\Sigma']^2 + [J(J+1) + S(S+1) - 2\Omega\Sigma]^2 \right. \\
& \quad \quad + [J(J+1) + S(S+1) - 2\Omega'\Sigma'] [J(J+1) + S(S+1) - 2\Omega\Sigma] \\
& \quad \left. + 4J(J+1)(2J+1)S(S+1)(2S+1) \begin{pmatrix} J & 1 & J \\ -\Omega' & q & \Omega \end{pmatrix}^2 \begin{pmatrix} S & 1 & S \\ -\Sigma' & q & \Sigma \end{pmatrix}^2 \right] \right\}. \tag{B.12}
\end{aligned}$$

(12) Centrifugal distortion effect to spin-molecular rotation coupling

$$\begin{aligned}
& \langle L\Lambda', S\Sigma', J'\Omega' M'_{J'}, I M'_I | \gamma_D \left\{ T^1(\hat{\mathbf{J}} - \hat{\mathbf{S}}) \cdot T^1(\hat{\mathbf{S}}) \right\} \hat{\mathbf{N}}^2 | L\Lambda, S\Sigma, J\Omega M_J, I M_I \rangle \\
& = \gamma_D \delta_{\Lambda, \Lambda'} \delta_{J, J'} \delta_{M_J, M'_{J'}} \delta_{M_I, M'_I} \\
& \times \left\{ \delta_{\Omega, \Omega'} \delta_{\Sigma, \Sigma'} [\Omega\Sigma - S(S+1)] [J(J+1) + S(S+1) - 2\Omega\Sigma] \right. \\
& \quad \left. + [J(J+1) + 3S(S+1) - 2\Omega'\Sigma' - 2\Omega\Sigma] \right\}
\end{aligned}$$

$$\begin{aligned}
& \times (-1)^{J-\Omega'+S-\Sigma'} \sqrt{J(J+1)(2J+1)S(S+1)(2S+1)} \sum_{q=\pm 1} \begin{pmatrix} J & 1 & J \\ -\Omega' & q & \Omega \end{pmatrix} \begin{pmatrix} S & 1 & S \\ -\Sigma' & q & \Sigma \end{pmatrix} \\
& - 2\delta_{\Omega,\Omega'}\delta_{\Sigma,\Sigma'} J(J+1)(2J+1)S(S+1)(2S+1) \\
& \times \sum_{q=\pm 1} \theta(3/2 - |\Omega - q|) \left[\begin{pmatrix} J & 1 & J \\ -\Omega & q & \Omega - q \end{pmatrix} \begin{pmatrix} S & 1 & S \\ -\Sigma & q & \Sigma - q \end{pmatrix} \right]^2 \}. \tag{B.13}
\end{aligned}$$

(13) Centrifugal distortion effect to Λ -doubling term (I)

- $-Q_D$ term

$$\begin{aligned}
& - \langle L\Lambda', S\Sigma', J'\Omega' M'_{J'}, I M'_I | \sum_{q=\pm 1} e^{-2iq\phi} \frac{Q_D}{2} \left[T_{2q}^2(\hat{\mathbf{J}}, \hat{\mathbf{J}}) \hat{\mathbf{N}}^2 + \hat{\mathbf{N}}^2 T_{2q}^2(\hat{\mathbf{J}}, \hat{\mathbf{J}}) \right] | L\Lambda, S\Sigma, J\Omega M_J, I M_I \rangle \\
& = \frac{Q_D}{4\sqrt{6}} \delta_{J,J'} \delta_{M_J, M'_{J'}} \delta_{M_I, M'_I} \sqrt{(2J-1)2J(2J+1)(2J+2)(2J+3)} \sum_{q=\pm 1} \delta_{\Lambda', \Lambda-2q} \\
& \times \left\{ \delta_{\Sigma, \Sigma'} [2J(J+1) + 2S(S+1) - 2(\Omega' + \Omega)\Sigma] (-1)^{J-\Omega'} \begin{pmatrix} J & 2 & J \\ -\Omega' & -2q & \Omega \end{pmatrix} \right. \\
& - 2(-1)^{S-\Sigma'} \sqrt{J(J+1)(2J+1)S(S+1)(2S+1)} \\
& \times \sum_{q'=\pm 1} \left[\begin{pmatrix} J & 2 & J \\ -\Omega' & -2q & \Omega' + 2q \end{pmatrix} \begin{pmatrix} J & 1 & J \\ -\Omega' - 2q & q' & \Omega \end{pmatrix} \begin{pmatrix} S & 1 & S \\ -\Sigma' & q' & \Sigma \end{pmatrix} \theta(3/2 - |\Omega' + 2q|) \right. \\
& \left. \left. - \begin{pmatrix} J & 1 & J \\ -\Omega' & q' & \Omega' - q' \end{pmatrix} \begin{pmatrix} S & 1 & S \\ -\Sigma' & q' & \Sigma \end{pmatrix} \begin{pmatrix} J & 2 & J \\ -\Omega' + q' & -2q & \Omega \end{pmatrix} \theta(3/2 - |\Omega' - q'|) \right] \}. \tag{B.14}
\end{aligned}$$

- $(P_D + 2Q_D)$ term

$$\begin{aligned}
& \langle L\Lambda', S\Sigma', J'\Omega' M'_{J'}, I M'_I | \frac{P_D + 2Q_D}{2} \sum_{q=\pm 1} e^{-2iq\phi} \left[T_{2q}^2(\hat{\mathbf{J}}, \hat{\mathbf{S}}) \hat{\mathbf{N}}^2 + \hat{\mathbf{N}}^2 T_{2q}^2(\hat{\mathbf{J}}, \hat{\mathbf{S}}) \right] | L\Lambda, S\Sigma, J\Omega M_J, I M_I \rangle \\
& = \frac{P_D + 2Q_D}{2} \delta_{J,J'} \delta_{M_J, M'_{J'}} \delta_{M_I, M'_I} \sqrt{J(J+1)(2J+1)S(S+1)(2S+1)} \sum_{q=\pm 1} \delta_{\Lambda', \Lambda-2q} \\
& \times \left\{ (-1)^{J-\Omega'+S-\Sigma'} [2J(J+1) + 2S(S+1) - 2\Omega'\Sigma' - 2\Omega\Sigma] \begin{pmatrix} J & 1 & J \\ -\Omega' & -q & \Omega \end{pmatrix} \begin{pmatrix} S & 1 & S \\ -\Sigma' & q & \Sigma \end{pmatrix} \right. \\
& - 2\delta_{\Sigma, \Sigma'} \sqrt{J(J+1)(2J+1)S(S+1)(2S+1)} \theta(3/2 - |\Omega' + q|) \\
& \times \begin{pmatrix} J & 1 & J \\ -\Omega' & -q & \Omega' + q \end{pmatrix} \begin{pmatrix} J & 1 & J \\ -\Omega' - q & -q & \Omega \end{pmatrix} \\
& \left. \times \left[\begin{pmatrix} S & 1 & S \\ -\Sigma & q & \Sigma - q \end{pmatrix} \begin{pmatrix} S & 1 & S \\ -\Sigma + q & -q & \Sigma \end{pmatrix} + \begin{pmatrix} S & 1 & S \\ -\Sigma & -q & \Sigma + q \end{pmatrix} \begin{pmatrix} S & 1 & S \\ -\Sigma - q & q & \Sigma \end{pmatrix} \right] \right\}. \tag{B.15}
\end{aligned}$$

(14) Centrifugal distortion effect to Λ -doubling term (II)

- $-Q_H$ term

$$\begin{aligned}
& - \langle L\Lambda', S\Sigma', J'\Omega' M'_{J'}, I M'_I | \sum_{q=\pm 1} e^{-2iq\phi} Q_H \frac{1}{2} \left[T_{2q}^2(\hat{\mathbf{J}}, \hat{\mathbf{J}}) (\hat{\mathbf{N}}^2)^2 + (\hat{\mathbf{N}}^2)^2 T_{2q}^2(\hat{\mathbf{J}}, \hat{\mathbf{J}}) \right] | L\Lambda, S\Sigma, J\Omega M_J, I M_I \rangle \\
& = \frac{Q_H}{4\sqrt{6}} \delta_{J,J'} \delta_{M_J, M'_{J'}} \delta_{M_I, M'_I} \sqrt{(2J-1)2J(2J+1)(2J+2)(2J+3)} \sum_{q=\pm 1} \delta_{\Lambda', \Lambda-2q} \\
& \times \left\{ \delta_{\Sigma, \Sigma'} (-1)^{J-\Omega'} \left[[J(J+1) + S(S+1) - 2\Omega'\Sigma']^2 + [J(J+1) + S(S+1) - 2\Omega\Sigma]^2 \right] \begin{pmatrix} J & 2 & J \\ -\Omega' & -2q & \Omega \end{pmatrix} \right.
\end{aligned}$$

$$\begin{aligned}
& + 4\delta_{\Sigma,\Sigma'}(-1)^{J-\Omega'}J(J+1)(2J+1)S(S+1)(2S+1)\begin{pmatrix} J & 2 & J \\ -\Omega' & -2q & \Omega \end{pmatrix}\sum_{q'=\pm 1}\begin{pmatrix} S & 1 & S \\ -\Sigma & q' & \Sigma-q' \end{pmatrix}^2 \\
& \times \left[\begin{pmatrix} J & 1 & J \\ -\Omega' & q' & \Omega'-q' \end{pmatrix}^2\theta(3/2-|\Omega'-q'|) + \begin{pmatrix} J & 1 & J \\ -\Omega & q' & \Omega-q' \end{pmatrix}^2\theta(3/2-|\Omega-q'|) \right] \\
& - 2(-1)^{S-\Sigma'}\sqrt{J(J+1)(2J+1)S(S+1)(2S+1)} \\
& \times \left[[2J(J+1)+2S(S+1)-2(\Omega'+2q)\Sigma'-2\Omega\Sigma]\begin{pmatrix} J & 2 & J \\ -\Omega' & -2q & \Omega'+2q \end{pmatrix}\theta(3/2-|\Omega'+2q|) \right. \\
& \quad \times \sum_{q'=\pm 1}\begin{pmatrix} J & 1 & J \\ -\Omega'-2q & q' & \Omega \end{pmatrix}\begin{pmatrix} S & 1 & S \\ -\Sigma' & q' & \Sigma \end{pmatrix} \\
& \quad \left. - [2J(J+1)+2S(S+1)-2\Omega'\Sigma'-2(\Omega-2q)\Sigma]\begin{pmatrix} J & 2 & J \\ -\Omega+2q & -2q & \Omega \end{pmatrix}\theta(3/2-|\Omega-2q|) \right. \\
& \quad \left. \times \sum_{q'=\pm 1}\begin{pmatrix} J & 1 & J \\ -\Omega' & q' & \Omega-2q \end{pmatrix}\begin{pmatrix} S & 1 & S \\ -\Sigma' & q' & \Sigma \end{pmatrix} \right] \Big\}. \tag{B.16}
\end{aligned}$$

• ($P_H + 2Q_H$) term

$$\begin{aligned}
& \langle L\Lambda', S\Sigma', J'\Omega' M'_{J'}, I M'_I | \sum_{q=\pm 1} e^{-2iq\phi} \frac{P_H + 2Q_H}{2} \left[T_{2q}^2(\hat{\mathbf{J}}, \hat{\mathbf{S}})(\hat{\mathbf{N}}^2)^2 + (\hat{\mathbf{N}}^2)^2 T_{2q}^2(\hat{\mathbf{J}}, \hat{\mathbf{S}}) \right] | L\Lambda, S\Sigma, J\Omega M_J, I M_I \rangle \\
& = \frac{P_H + 2Q_H}{2} \delta_{J,J'} \delta_{M_J, M'_{J'}} \delta_{M_I, M'_I} \sqrt{J(J+1)(2J+1)S(S+1)(2S+1)} \sum_{q=\pm 1} \delta_{\Lambda', \Lambda-2q} \\
& \times \left\{ (-1)^{J-\Omega'+S-\Sigma'} \begin{pmatrix} J & 1 & J \\ -\Omega' & -q & \Omega \end{pmatrix} \begin{pmatrix} S & 1 & S \\ -\Sigma' & q & \Sigma \end{pmatrix} \right. \\
& \quad \times \left[[J(J+1)+S(S+1)-2\Omega'\Sigma']^2 + [J(J+1)+S(S+1)-2\Omega\Sigma]^2 \right] \\
& \quad + 4(-1)^{J-\Omega'+S-\Sigma'} J(J+1)(2J+1)S(S+1)(2S+1) \begin{pmatrix} J & 1 & J \\ -\Omega' & -q & \Omega \end{pmatrix} \begin{pmatrix} S & 1 & S \\ -\Sigma' & q & \Sigma \end{pmatrix} \\
& \quad \times \sum_{q'=\pm 1} \left[\begin{pmatrix} J & 1 & J \\ -\Omega' & q' & \Omega'-q' \end{pmatrix}^2 \begin{pmatrix} S & 1 & S \\ -\Sigma' & q' & \Sigma'-q' \end{pmatrix}^2 \theta(3/2-|\Omega'-q'|) \right. \\
& \quad \left. + \begin{pmatrix} J & 1 & J \\ -\Omega & q' & \Omega-q' \end{pmatrix}^2 \begin{pmatrix} S & 1 & S \\ -\Sigma & q' & \Sigma-q' \end{pmatrix}^2 \theta(3/2-|\Omega-q'|) \right] \\
& \quad - 2\delta_{\Sigma,\Sigma'} \sqrt{J(J+1)(2J+1)S(S+1)(2S+1)} \\
& \quad \times \left[[2J(J+1)+2S(S+1)-2(\Omega'+q)(\Sigma-q)-2\Omega\Sigma] \begin{pmatrix} J & 1 & J \\ -\Omega' & -q & \Omega'+q \end{pmatrix} \begin{pmatrix} S & 1 & S \\ -\Sigma & q & \Sigma-q \end{pmatrix} \right]^2 \\
& \quad \times \theta(3/2-|\Omega'+q|) \begin{pmatrix} J & 1 & J \\ -\Omega'-q & -q & \Omega \end{pmatrix} \\
& \quad + [2J(J+1)+2S(S+1)-2\Omega'\Sigma-2(\Omega-q)(\Sigma+q)] \begin{pmatrix} J & 1 & J \\ -\Omega+q & -q & \Omega \end{pmatrix} \\
& \quad \left. \times \theta(3/2-|\Omega-q|) \begin{pmatrix} J & 1 & J \\ -\Omega' & -q & \Omega-q \end{pmatrix} \begin{pmatrix} S & 1 & S \\ -\Sigma & -q & \Sigma+q \end{pmatrix}^2 \right] \Big\}. \tag{B.17}
\end{aligned}$$

(15) Centrifugal distortion effect to magnetic hyperfine interaction

$$\begin{aligned}
& \langle L\Lambda', S\Sigma', J'\Omega' M'_{J'}, I M'_I | d_D \sum_{q=\pm 1} e^{-2iq\phi} \frac{1}{2} \left[T_{2q}^2(\hat{\mathbf{I}}, \hat{\mathbf{S}}) \hat{\mathbf{N}}^2 + \hat{\mathbf{N}}^2 T_{2q}^2(\hat{\mathbf{I}}, \hat{\mathbf{S}}) \right] | L\Lambda, S\Sigma, J\Omega M_J, I M_I \rangle \\
&= \frac{d_D}{2} \sqrt{(2J' + 1)(2J + 1)I(I + 1)(2I + 1)S(S + 1)(2S + 1)} \\
&\times (-1)^{I - M'_I} \sum_{p=0, \pm 1} (-1)^p \begin{pmatrix} J' & 1 & J \\ -M'_{J'} & p & M_J \end{pmatrix} \begin{pmatrix} I & 1 & I \\ -M'_I & -p & M_I \end{pmatrix} \sum_{q=\pm 1} \delta_{\Lambda', \Lambda - 2q} \\
&\times \left\{ [J'(J' + 1) + J(J + 1) + 2S(S + 1) - 2\Omega'\Sigma' - 2\Omega\Sigma] (-1)^{M'_{J'} - \Omega' + S - \Sigma'} \begin{pmatrix} J' & 1 & J \\ -\Omega' & -q & \Omega \end{pmatrix} \begin{pmatrix} S & 1 & S \\ -\Sigma' & q & \Sigma \end{pmatrix} \right. \\
&\quad + 2\delta_{\Sigma, \Sigma'} \theta(3/2 - |\Omega' + q|) (-1)^{J' + M'_{J'}} \sqrt{S(S + 1)(2S + 1)} \\
&\quad \times \left[\sqrt{J'(J' + 1)(2J' + 1)} \begin{pmatrix} J' & 1 & J' \\ -\Omega' & -q & \Omega' + q \end{pmatrix} \begin{pmatrix} S & 1 & S \\ -\Sigma & -q & \Sigma + q \end{pmatrix} \right. \\
&\quad \times \begin{pmatrix} J' & 1 & J \\ -\Omega' - q & -q & \Omega \end{pmatrix} \begin{pmatrix} S & 1 & S \\ -\Sigma - q & q & \Sigma \end{pmatrix} \\
&\quad \left. + (-1)^{J - J'} \sqrt{J(J + 1)(2J + 1)} \begin{pmatrix} J' & 1 & J \\ -\Omega' & -q & \Omega' + q \end{pmatrix} \begin{pmatrix} S & 1 & S \\ -\Sigma & q & \Sigma - q \end{pmatrix} \right. \\
&\quad \left. \times \begin{pmatrix} J & 1 & J \\ -\Omega' - q & -q & \Omega \end{pmatrix} \begin{pmatrix} S & 1 & S \\ -\Sigma + q & -q & \Sigma \end{pmatrix} \right] \left. \right\}. \tag{B.18}
\end{aligned}$$

(16) Orbital Zeeman effect

$$\begin{aligned}
& \langle L\Lambda', S\Sigma', J'\Omega' M'_{J'}, I M'_I | g'_L \mu_B B_Z T_{p=0}^1(\hat{\mathbf{L}}) | L\Lambda, S\Sigma, J\Omega M_J, I M_I \rangle \\
&= g'_L \mu_B B_Z \delta_{\Lambda, \Lambda'} \delta_{\Sigma, \Sigma'} \delta_{M_I, M'_I} \Lambda (-1)^{M'_{J'} - \Omega'} \sqrt{(2J' + 1)(2J + 1)} \begin{pmatrix} J' & 1 & J \\ -\Omega' & 0 & \Omega \end{pmatrix} \begin{pmatrix} J' & 1 & J \\ -M'_{J'} & 0 & M_J \end{pmatrix}. \tag{B.19}
\end{aligned}$$

(17) electronic spin isotropic contribution to Zeeman effect

$$\begin{aligned}
& \langle L\Lambda', S\Sigma', J'\Omega' M'_{J'}, I M'_I | g_S \mu_B B_Z T_{p=0}^1(\hat{\mathbf{S}}) | L\Lambda, S\Sigma, J\Omega M_J, I M_I \rangle \\
&= g_S \mu_B B_Z \delta_{\Lambda, \Lambda'} \delta_{M_I, M'_I} (-1)^{M'_{J'} - \Omega' + S - \Sigma'} \sqrt{(2J' + 1)(2J + 1)S(S + 1)(2S + 1)} \begin{pmatrix} J' & 1 & J \\ -M'_{J'} & 0 & M_J \end{pmatrix} \\
&\times \sum_{q=0, \pm 1} \begin{pmatrix} J' & 1 & J \\ -\Omega' & q & \Omega \end{pmatrix} \begin{pmatrix} S & 1 & S \\ -\Sigma' & q & \Sigma \end{pmatrix}. \tag{B.20}
\end{aligned}$$

(18) Rotational magnetic moment contribution to Zeeman effect

$$\begin{aligned}
& - \langle L\Lambda', S\Sigma', J'\Omega' M'_{J'}, I M'_I | g_r \mu_B B_Z T_{p=0}^1(\hat{\mathbf{J}} - \hat{\mathbf{L}} - \hat{\mathbf{S}}) | L\Lambda, S\Sigma, J\Omega M_J, I M_I \rangle \\
&= -g_r \mu_B B_Z \delta_{\Lambda, \Lambda'} \delta_{\Sigma, \Sigma'} \delta_{J, J'} \delta_{\Omega, \Omega'} \delta_{M_J, M'_{J'}} \delta_{M_I, M'_I} M_J \\
&\quad + g_r \mu_B B_Z \delta_{\Lambda, \Lambda'} \delta_{\Sigma, \Sigma'} \delta_{M_I, M'_I} \Lambda (-1)^{M'_{J'} - \Omega'} \sqrt{(2J' + 1)(2J + 1)} \begin{pmatrix} J' & 1 & J \\ -\Omega' & 0 & \Omega \end{pmatrix} \begin{pmatrix} J' & 1 & J \\ -M'_{J'} & 0 & M_J \end{pmatrix} \\
&\quad + g_r \mu_B B_Z \delta_{\Lambda, \Lambda'} \delta_{M_I, M'_I} (-1)^{M'_{J'} - \Omega' + S - \Sigma'} \sqrt{(2J' + 1)(2J + 1)S(S + 1)(2S + 1)} \begin{pmatrix} J' & 1 & J \\ -M'_{J'} & 0 & M_J \end{pmatrix} \\
&\quad \times \sum_{q_1=0, \pm 1} \begin{pmatrix} J' & 1 & J \\ -\Omega' & q_1 & \Omega \end{pmatrix} \begin{pmatrix} S & 1 & S \\ -\Sigma' & q_1 & \Sigma \end{pmatrix}. \tag{B.21}
\end{aligned}$$

(19) Nuclear spin Zeeman effect

$$\begin{aligned}
& -\langle L\Lambda', S\Sigma', J'\Omega' M'_{J'}, I M'_I | g_N \mu_N B_Z T_{p=0}^1(\hat{\mathbf{I}}) | L\Lambda, S\Sigma, J\Omega M_J, I M_I \rangle \\
& = -g_N \mu_N B_Z \delta_{\Lambda, \Lambda'} \delta_{\Sigma, \Sigma'} \delta_{J, J'} \delta_{\Omega, \Omega'} \delta_{M_J, M'_{J'}} \delta_{M_I, M'_I} M_I,
\end{aligned} \tag{B.22}$$

where the g-factor of Hydrogen nucleus is $g_N = 2.792847$, the nuclear magneton is $\mu_N = e\hbar/m_p = 5.05078343(43) \times 10^{-27}$ J/T, and Bohr magneton is $\mu_B = e\hbar/m_e = 9.27400915(23) \times 10^{-24}$ J/T, which yields $\mu_N/\mu_B \simeq 5.44617 \times 10^{-4}$. We also remark that $1\mu_B \times 1$ Gauss $\simeq 1.39962$ MHz.

(20) electronic spin anisotropic contribution to Zeeman effect

$$\begin{aligned}
& \langle L\Lambda', S\Sigma', J'\Omega' M'_{J'}, I M'_I | g_\ell \mu_B B_Z \sum_{q=\pm 1} \mathcal{D}_{0,q}^{(1)*}(\omega) T_q^1(\hat{\mathbf{S}}) | L\Lambda, S\Sigma, J\Omega M_J, I M_I \rangle \\
& = g_\ell \mu_B B_Z \delta_{\Lambda, \Lambda'} \delta_{M_I, M'_I} (-1)^{M'_{J'} - \Omega' + S - \Sigma'} \sqrt{(2J' + 1)(2J + 1)S(S + 1)(2S + 1)} \begin{pmatrix} J' & 1 & J \\ -M'_{J'} & 0 & M_J \end{pmatrix} \\
& \quad \times \sum_{q=\pm 1} \begin{pmatrix} J' & 1 & J \\ -\Omega' & q & \Omega \end{pmatrix} \begin{pmatrix} S & 1 & S \\ -\Sigma' & q & \Sigma \end{pmatrix}.
\end{aligned} \tag{B.23}$$

(21) Parity-dependent and non-cylindrical contribution to Zeeman effect (I)

$$\begin{aligned}
& \langle L\Lambda', S\Sigma', J'\Omega' M'_{J'}, I M'_I | g'_\ell \mu_B B_Z \sum_{q=\pm 1} e^{-2iq\phi} \mathcal{D}_{0,-q}^{(1)*}(\omega) T_q^1(\hat{\mathbf{S}}) | L\Lambda, S\Sigma, J\Omega M_J, I M_I \rangle \\
& = -g'_\ell \mu_B B_Z \delta_{M_I, M'_I} (-1)^{M'_{J'} - \Omega' + S - \Sigma'} \sqrt{(2J' + 1)(2J + 1)S(S + 1)(2S + 1)} \begin{pmatrix} J' & 1 & J \\ -M'_{J'} & 0 & M_J \end{pmatrix} \\
& \quad \times \sum_{q=\pm 1} \delta_{\Lambda', \Lambda - 2q} \begin{pmatrix} J' & 1 & J \\ -\Omega' & -q & \Omega \end{pmatrix} \begin{pmatrix} S & 1 & S \\ -\Sigma' & q & \Sigma \end{pmatrix}.
\end{aligned} \tag{B.24}$$

(22) Parity-dependent and non-cylindrical contribution to Zeeman effect (II)

$$\begin{aligned}
& -\langle L\Lambda', S\Sigma', J'\Omega' M'_{J'}, I M'_I | g'_r \mu_B B_Z \sum_{q=\pm 1} \sum_{p=0, \pm 1} e^{-2iq\phi} (-1)^p \mathcal{D}_{-p,-q}^{(1)*}(\omega) T_p^1(\hat{\mathbf{J}} - \hat{\mathbf{S}}) \mathcal{D}_{0,-q}^{(1)*}(\omega) | L\Lambda, S\Sigma, J\Omega M_J, I M_I \rangle \\
& = g'_r \mu_B B_Z \delta_{M_I, M'_I} \sqrt{(2J' + 1)(2J + 1)} \begin{pmatrix} J' & 1 & J \\ -M'_{J'} & 0 & M_J \end{pmatrix} \sum_{q=\pm 1} \delta_{\Lambda', \Lambda - 2q} \\
& \quad \times \left\{ \delta_{\Sigma, \Sigma'} (-1)^{J' + M'_{J'}} \sqrt{J'(J' + 1)(2J' + 1)} \begin{pmatrix} J' & 1 & J' \\ -\Omega' & -q & \Omega' + q \end{pmatrix} \begin{pmatrix} J' & 1 & J \\ -\Omega' - q & -q & \Omega \end{pmatrix} \theta(3/2 - |\Omega' + q|) \right. \\
& \quad \left. + (-1)^{M'_{J'} - \Omega' + S - \Sigma'} \sqrt{S(S + 1)(2S + 1)} \begin{pmatrix} J' & 1 & J \\ -\Omega' & -q & \Omega \end{pmatrix} \begin{pmatrix} S & 1 & S \\ -\Sigma' & q & \Sigma \end{pmatrix} \right\}.
\end{aligned} \tag{B.25}$$

(23) Stark effect

$$\begin{aligned}
& \langle L\Lambda', S\Sigma', J'\Omega' M'_{J'}, I M'_I | -\hat{\mathbf{d}} \cdot \mathbf{E}_{\text{DC}} | L\Lambda, S\Sigma, J\Omega M_J, I M_I \rangle \\
& = -\mu_z^{(e)} E_{\text{DC}} \delta_{\Lambda, \Lambda'} \delta_{\Sigma, \Sigma'} \delta_{M_I, M'_I} (-1)^{M'_{J'} - \Omega'} \sqrt{(2J' + 1)(2J + 1)} \begin{pmatrix} J' & 1 & J \\ -\Omega' & 0 & \Omega \end{pmatrix} \\
& \quad \times \sum_{p=0, \pm 1} d_{p,0}^{(1)}(\theta_{BE}) \begin{pmatrix} J' & 1 & J \\ -M'_{J'} & p & M_J \end{pmatrix}.
\end{aligned} \tag{B.26}$$

References

- [1] G. C. Dousmanis, T. M. Sanders, and C. H. Townes. Microwave spectra of the free radicals OH and OD. *Phys. Rev.*, 100:1735–1754, Dec 1955.

- [2] H. E. Radford. Microwave Zeeman effect of free hydroxyl radicals. *Phys. Rev.*, 122:114–130, Apr 1961.
- [3] J. J. ter Meulen and A. Dymanus. Beam maser measurements of the ground states transition frequencies of OH. *Astrophys. J.*, 172:L21, 1972.
- [4] S. Weinreb, A. H. Barrett, M. L. Meeks, and J. C. Henry. Radio observations of oh in the interstellar medium. *Nature*, 200(4909):829–831, 11 1963.
- [5] H Weaver, D. R. W. Williams, N. H. Dieter, and W. T. Lum. Observations of a strong unidentified microwave line and of emission from the oh molecule. *Nature*, 208(5005):29–31, 10 1965.
- [6] Moshe Elitzur. Physical characteristics of astronomical masers. *Rev. Mod. Phys.*, 54:1225–1260, Oct 1982.
- [7] Benjamin K. Stuhl, Matthew T. Hummon, Mark Yeo, Goulven Quemener, John L. Bohn, and Jun Ye. Evaporative cooling of the dipolar hydroxyl radical. *Nature*, 492(7429):396–400, 12 2012.
- [8] J. M. Brown, M. Kaise, C. M. L. Kerr, and D. J. Milton. A determination of fundamental Zeeman parameters for the OH radical. *Mol. Phys.*, 36:553, 1978.
- [9] J. M. Brown, C. M. L. Kerr, and F. D. Wayne. The far-infrared laser magnetic resonance — spectrum of the OH radical. *J. Mol. Spectrosc.*, 86:544, 1981.
- [10] J. A. Coxon. Optimum molecular constants and term values for the $X^2\Pi(v \leq 5)$ and $A^2\Sigma^+(v \leq 3)$ states of OH. *Canadian Journal of Physics*, 58(7):933–949, 1980.
- [11] Alexandr V. Avdeenkov and John L. Bohn. Collisional dynamics of ultracold OH molecules in an electrostatic field. *Phys. Rev. A*, 66:052718, Nov 2002.
- [12] Christopher Ticknor and John L. Bohn. Influence of magnetic fields on cold collisions of polar molecules. *Phys. Rev. A*, 71:022709, Feb 2005.
- [13] Benjamin K. Stuhl, Mark Yeo, Brian C. Sawyer, Matthew T. Hummon, and Jun Ye. Microwave state transfer and adiabatic dynamics of magnetically trapped polar molecules. *Phys. Rev. A*, 85:033427, Mar 2012.
- [14] John L. Bohn and Goulven Quémener. Dipolar radicals in crossed electric and magnetic fields. *Mol. Phys.*, 111(12-13):1931–1938, 2013.
- [15] Goulven Quémener and John L. Bohn. Ultracold molecular collisions in combined electric and magnetic fields. *Phys. Rev. A*, 88:012706, Jul 2013.
- [16] M. Bhattacharya, Z. Howard, and M. Kleinert. Ground-state OH molecule in combined electric and magnetic fields: analytic solution of the effective Hamiltonian. *Phys. Rev. A*, 88:012503, Jul 2013.
- [17] T. Koch, T. Lahaye, J. Metz, B. Frohlich, A. Griesmaier, and T. Pfau. Stabilization of a purely dipolar quantum gas against collapse. *Nat Phys*, 4(3):218–222, 03 2008.
- [18] Mingwu Lu, Nathaniel Q. Burdick, Seo Ho Youn, and Benjamin L. Lev. Strongly dipolar Bose-Einstein condensate of Dysprosium. *Phys. Rev. Lett.*, 107:190401, Oct 2011.
- [19] K. Aikawa, A. Frisch, M. Mark, S. Baier, A. Rietzler, R. Grimm, and F. Ferlaino. Bose-Einstein condensation of Erbium. *Phys. Rev. Lett.*, 108:210401, May 2012.
- [20] S. Yi and H. Pu. Spontaneous spin textures in dipolar spinor condensates. *Phys. Rev. Lett.*, 97:020401, Jul 2006.
- [21] Yuki Kawaguchi, Hiroki Saito, and Masahito Ueda. Can spinor dipolar effects be observed in Bose-Einstein condensates? *Phys. Rev. Lett.*, 98:110406, Mar 2007.
- [22] M. Vengalattore, S. R. Leslie, J. Guzman, and D. M. Stamper-Kurn. Spontaneously modulated spin textures in a dipolar spinor Bose-Einstein condensate. *Phys. Rev. Lett.*, 100:170403, May 2008.
- [23] B. Pasquiou, G. Bismut, Q. Beaufils, A. Crubellier, E. Maréchal, P. Pedri, L. Vernac, O. Gorceix, and B. Laburthe-Tolra. Control of dipolar relaxation in external fields. *Phys. Rev. A*, 81:042716, Apr 2010.
- [24] Yuki Kawaguchi, Hiroki Saito, and Masahito Ueda. Einstein-de Haas effect in dipolar Bose-Einstein condensates. *Phys. Rev. Lett.*, 96:080405, Mar 2006.
- [25] L. Santos and T. Pfau. Spin-3 Chromium Bose-Einstein condensates. *Phys. Rev. Lett.*, 96:190404, May 2006.
- [26] Takahiko Miyakawa, Takaaki Sogo, and Han Pu. Phase-space deformation of a trapped dipolar Fermi gas. *Phys. Rev. A*, 77:061603, Jun 2008.
- [27] Benjamin M. Fregoso and Eduardo Fradkin. Ferronematic ground state of the dilute dipolar Fermi gas. *Phys. Rev. Lett.*, 103:205301, Nov 2009.
- [28] Kenji Maeda, Tetsuo Hatsuda, and Gordon Baym. Antiferromagnetic ground state of two-component dipolar Fermi gases: an analog of meson condensation in nuclear matter. *Phys. Rev. A*, 87:021604, Feb 2013.
- [29] Bo Yan, Steven A. Moses, Bryce Gadway, Jacob P. Covey, Kaden R. A. Hazzard, Ana Maria Rey, Deborah S. Jin, and Jun Ye. Observation of dipolar spin-exchange interactions with lattice-confined polar molecules. *Nature*, 501(7468):521–525, 09 2013.
- [30] Benjamin Pasquiou, Alex Bayerle, Slava M. Tzanova, Simon Stellmer, Jacek Szczepkowski, Mark Parigger, Rudolf

- Grimm, and Florian Schreck. Quantum degenerate mixtures of Strontium and Rubidium atoms. *Phys. Rev. A*, 88:023601, Aug 2013.
- [31] E. S. Shuman, J. F. Barry, and D. DeMille. Laser cooling of a diatomic molecule. *Nature*, 467(7317):820–823, 10 2010.
- [32] M. L. Wall, K. Maeda, and L. D. Carr. Simulating quantum magnets with symmetric top molecules. *Ann. Phys.*, 525:845–865, 2013.
- [33] M. Born and R. Oppenheimer. Zur quantentheorie der molekeln. *Ann. Phys.*, 84:457–484, 1927.
- [34] Gordon Baym. *Lectures on Quantum Mechanics*. Addison-Wesley, 1969.
- [35] D. R. Hartree. The wave mechanics of an atom with a non-Coulomb central field. Part I. Theory and methods. *Proc. Cambridge Phil. Soc.*, 24:89–110, 1928.
- [36] D. R. Hartree. The wave mechanics of an atom with a non-Coulomb central field. Part II. Some results and discussion. *Proc. Cambridge Phil. Soc.*, 24:111–132, 1928.
- [37] V. Fock. Näherungsmethode zur Lösung des quantenmechanischen Mehrkörperproblems. *Z. Phys.*, 61:126–148, 1930.
- [38] V. Fock. „Selfconsistent field“ mit Austausch für Natrium. *Z. Phys.*, 62:795–805, 1930.
- [39] John C. Slater. *Quantum Theory of Molecules and Solids: Volume 1, Electronic Structure of Molecules*. McGraw-Hill, 1963.
- [40] J. H. Brown and A. Carrington. *Rotational Spectroscopy of Diatomic Molecules*. Cambridge University Press, 2003.
- [41] Robert S. Mulliken and Andrew Christy. Λ -type doubling and electron configurations in diatomic molecules. *Phys. Rev.*, 38:87–119, Jul 1931.
- [42] Richard N. Zare. *Angular Momentum: Understanding Spatial Aspects in Chemistry and Physics*. Wiley, 1988.
- [43] J. M. Brown, E. A. Colbourn, J. K. G. Watson, and F. D. Wayne. An effective Hamiltonian for diatomic molecules — ab initio calculations of parameters of HCl. *J. Mol. Spectrosc.*, 74:294, 1979.
- [44] Eric R. Hudson, H. J. Lewandowski, Brian C. Sawyer, and Jun Ye. Cold molecule spectroscopy for constraining the evolution of the fine structure constant. *Phys. Rev. Lett.*, 96:143004, Apr 2006.
- [45] Benjamin L. Lev, Edmund R. Meyer, Eric R. Hudson, Brian C. Sawyer, John L. Bohn, and Jun Ye. Oh hyperfine ground state: From precision measurement to molecular qubits. *Phys. Rev. A*, 74:061402, Dec 2006.
- [46] K. I. Peterson, G. T. Fraser, and W. Klemperer. Electric dipole moment of $X^2\Pi$ OH and OD in several vibrational states. *Canadian Journal of Physics*, 62(12):1502–1507, 1984.
- [47] Karl F. Freed. Theory of the hyperfine structure of molecules: Application to $^3\Pi$ states of diatomic molecules intermediate between Hund’s cases (a) and (b). *J. Chem. Phys.*, 45(11), 1966.
- [48] Martin Gärttner, Juan J. Omiste, Peter Schmelcher, and Rosario González-Férez. Fine structure of open-shell diatomic molecules in combined electric and magnetic fields. *Molecular Physics*, 111(12-13):1865–1878, 2013.